Tectonophysics 589 (2013) 151–166

Contents lists available at ScienceDirect

Tectonophysics

journal homepage: www.elsevier.com/locate/tecto

Reconstruction of the Early Ordovician Famatinian arc through thermobarometry in lower and middle crustal exposures, Sierra de Valle Fértil, Argentina

Alina M. Tibaldi [a,b,*], Juan E. Otamendi [a,b], Eber A. Cristofolini [a,b], Ignacio Baliani [a,c], Barry A. Walker Jr. [d], George W. Bergantz [d]

[a] Universidad Nacional de Río Cuarto, Departamento de Geología, Argentina
[b] Consejo Nacional de Investigaciones Científicas y Técnicas, Argentina
[c] Agencia Nacional de Promoción Científica y Tecnológica, Argentina
[d] Department of Earth and Space Sciences, University of Washington, Seattle, WA 98195-1310, USA

ARTICLE INFO

Article history:
Received 7 May 2012
Received in revised form 27 December 2012
Accepted 29 December 2012
Available online 12 January 2013

Keywords:
Paleoarcs
Thermobarometry
Subduction zones
Famatinian arc

ABSTRACT

The crustal structure of the Famatinian paleoarc is reconstructed by determining the metamorphic crystallization P–T conditions from metasedimentary rocks at various structural levels in the Valle Fértil section. The bulk section exhibits a 15-km-thick arc crustal section. Thermobarometry shows that nested tonalitic and granodioritic plutons constructed the arc crust at depths <20 km. Dioritic and tonalitic bodies dominated between 20 and 25 km. The deepest exposed paleodepths are formed by cumulate and non-cumulate gabbroic rocks with interlayered quartz diorites that crystallized below 25 km. The boundary between the crust and the lithospheric mantle is not observed and would have been underneath a depth of 27 km. P–T estimates throughout the section reveals high geothermal gradients ranging from 25 °C/km to 35 °C/km. The thermal regime inferred for middle crustal levels is observed in active and ancient magmatic arcs. Thermophysical models predicting the array of retrieved P–T estimates require heat advection conducted by mafic magmas which either emplaced in the lower crust and/or intruded into middle crustal levels. Calculated seismic wave velocities of plutonic rocks dominating progressively deeper paleodepths are used to deduce the internal architecture of the Valle Fértil section. This result indicates that the Famatinian arc had a middle crustal structure very similar to that of the ancient Talkeetna arc; however a rapid increase of seismic wave velocities from ~6.3 km/s to >6.6 km/s is located at deeper depths in the Famatinian arc than in Talkeetna arc. The thickness of a crustal layer dominated by plutonic rocks with low seismic wave velocities (<6.2 km/s) is 10 km thinner than the crustal layer with similar physical properties in the Sierra Nevada batholith. A putative model for the whole Famatinian arc suggests a total crustal thickness between 30 and 35 km with three distinct layers.

1. Introduction

Arc magmatism is considered to be the fundamental process of post-Archean growth of the continental crust (Rudnick, 1995; Taylor and McLennan, 1985). Documenting the structure and petrology of arc crust is therefore critical to the understanding of crustal generation and evolution (Christensen and Mooney, 1995; Rudnick, 1995). An indirect window into deep crustal structure is afforded by geophysical investigations performed in active arcs (Calvert, 2011). By comparing seismic wave velocities of active arc crust with experimentally determined seismic velocities, rock types are inferred based on the seismic structure of an arc (e.g. Christensen and Mooney, 1995; Kitamura et al., 2003). In rare instances, however, arc crustal sections are actually exposed at the earth's surface, and the vertical and lateral distribution of the rock types and crustal rheology of arcs can be directly observed (DeBari and Greene, 2011; Miller and Snoke, 2009).

The Sierra de Valle Fértil is a deep, tilted crustal arc section comprising mainly magmatic rocks, with minor proportions of metasediments (Otamendi et al., 2009). Exposures reveal compositions ranging from gabbro to granodiorite with progressively more silicic rocks observed at higher levels in the section. U–Pb zircon crystallization ages of magmatic rocks from the Valle Fértil section indicate that this section was entirely constructed in ~20 My or less during the early Ordovician from ~485 to ~465 Ma (e.g. Ducea et al., 2010). Pressure–temperature determinations in the metasedimentary packages interlayered between plutonic rocks are utilized here to constrain the depth of emplacement of the plutonic rocks. Mineral assemblages preserved in the metasediments likely record metamorphic conditions at the time of Valle Fértil magmatism was active, as zircons from Valle Fértil igneous rocks and zircon rims from the metasediments record overlapping ages

* Corresponding author at: Universidad Nacional de Río Cuarto, Departamento de Geología, Argentina. Tel.: +54 358 4676198; fax: +54 358 4680280.
E-mail address: atibaldi@exa.unrc.edu.ar (A.M. Tibaldi).

0040-1951/$ – see front matter © 2013 Elsevier B.V. All rights reserved.
http://dx.doi.org/10.1016/j.tecto.2012.12.032

(Cristofolini et al., 2010; Ducea et al., 2010; Gallien et al., 2010; Rapela et al., 2001). Calculated P–T equilibrium conditions of metamorphic mineral assemblages in siliciclastic sedimentary protoliths such as metapelite and aluminous metagreywacke are fairly robust (e.g. Spear, 1993), allowing for the reconstruction of the vertical dimensions of the arc. We use the presented P–T estimates, along with exposed rock types, to construct a seismic wave velocity profile for the Sierra de Valle Fértil arc. We compare our model for the Valle Fértil crustal arc section with other cases of well-known ancient and active arcs.

2. Geological setting of the Famatinian magmatic arc

The Sierra de Valle Fértil is situated in the southern Famatinian magmatic arc. Famatinian magmatism began ca. 495 Ma when subduction was established along the western margin of western Gondwana (e.g. Pankhurst et al., 1998). The southern segment (28° to 38° Lat. S. present day coordinates) of the Famatinian arc (Fig. 1a) was closed during the middle Ordovician (beginning at ca. 465 Ma) when a continental microplate collided with the proto-Pacific Gondwana margin (Thomas and Astini, 1996). Subsequent Paleozoic and modern (Andean) uplift has exposed the Famatinian arc at various paleo-depths.

Between 28° and 33° S in areas where the Nazca plate is subducting beneath the South American plate at a relatively low angle (Barazangi and Isacks, 1976), the deepest plutonic levels of the Famatinian arc are currently exposed (Fig. 1a). To the north, between 22° and 28° S, the complementary Ordovician volcanics are interbedded with sedimentary rocks in the Altiplano-Puna region (Coira et al., 1999) and in Sierra de Famatina (Fanning et al., 2004). The host rocks of all the Famatinian plutonic batholiths are supracrustal sedimentary packages largely consisting of siliciclastic sediments with subordinate interlayered carbonate beds (Caminos, 1979). This regional-scale sedimentary sequence experienced metamorphism at a time broadly synchronous with the igneous activity, at either contact or regional metamorphic conditions (e.g. Pankhurst et al., 2000; and references therein). As progressively shallower levels of the Famatinian paleo-arc crust are exposed northward along strike, the host rock transitions into weakly- to non-metamorphosed sediments (Aceñolaza et al., 2000). Based on this correlation, late Neoproterozoic–early Cambrian thick turbiditic packages and late Cambrian shallow marine sediments are the most likely protoliths to the metamorphic units hosting the Famatinian arc plutonic rocks (e.g. Aceñolaza, 2003), whereas epizonal plutons in Sierra de Famatina and neighboring areas intruded into early Ordovician volcano-sedimentary sequences formed during the initial magmatic arc stage (Astini and Dávila, 2004; Toselli et al., 1996).

3. General local geological features from Sierras de Valle Fértil–La Huerta

Within the western belt of the currently exposed Famatinian magmatic arc (Fig. 1b), the Sierras de Valle Fértil–La Huerta contain well-exposed sections of the transition between lower and upper crustal levels (Otamendi et al., 2008). From west to east, the lithologic units display a progression towards shallower, more evolved igneous compositions and may be described as four units: (1) A complex layered mafic unit dominated by amphibole gabbronorites and quartz-poor diorites enclosing a suite of chilled mafic sills, dykes and enclaves, with local mafic/ultramafic olivine-bearing cumulate rocks; (2) an intermediate unit comprising an extremely heterogeneous suite of amphibole- and biotite-rich tonalites; (3) batholith-scale monzogranite to granodiorite, with local bodies of amphibole-bearing gabbros and leucogranite dikes; and (4) a supracrustal metasedimentary unit dominated by paragneissic migmatites (metatexite ≫ diatexite) that occurs either as km-long strips interlayered with igneous mafic and intermediate rocks or as

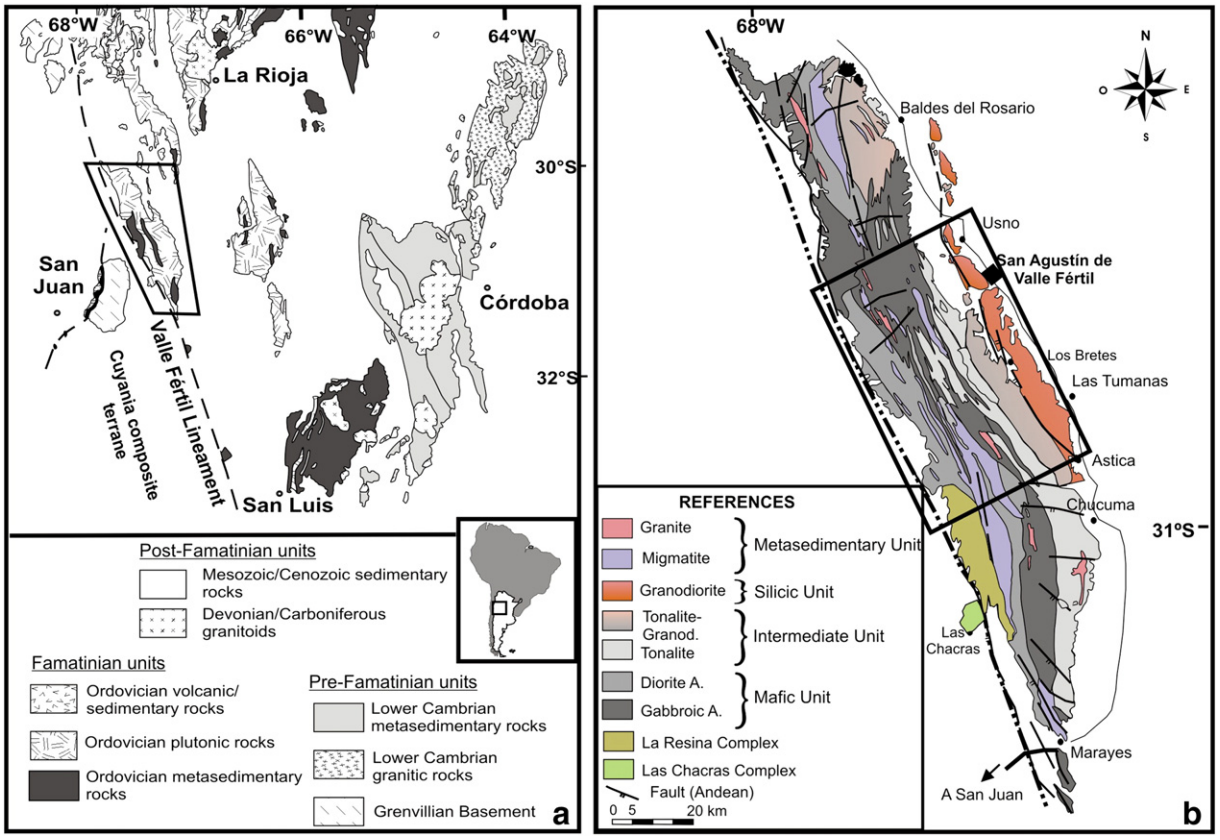

Fig. 1. a) Map showing the location of the study area with respect to the Pampean orogen, Famatinian magmatic arc and Cuyania and/or Precordillera terrane. Inset shows the location of the Sierras de Valle Fértil–La Huerta. b) Simplified geologic map of the Sierras de Valle Fértil–La Huerta. The study area is outlined.
a, map modified from Vujovich and Ramos (1999); b, simplified geologic map modified from the geological maps of Mirré (1976) and Vujovich et al. (1996, 1998).

widespread septa enclosed by gabbronorites and tonalites. Garnet-bearing leucogranites (products of partial melting of pelitic migmatites) occur widespread through the Sierra as tabular sills or lensoidal bodies. Metapelitic and semipelitic migmatites interlayered in the mafic unit record peak metamorphic pressures between 5.2 and 7.1 kbar at granulite-facies temperatures (Gallien et al., 2010; Otamendi et al., 2008; Tibaldi et al., 2011). The timing of magmatism in the Sierras de Valle Fértil–La Huerta is fairly well constrained between 482 and 468 Ma by U–Pb zircon geochronology (Ducea et al., 2010; Gallien et al., 2010; Pankhurst et al., 2000).

4. Petrography of metasedimentary migmatites

Metasedimentary migmatites in the Valle Fértil section are predominantly banded migmatites (metatexite) and are characterized by the development of discrete mesosomes and leucosomes ranging in thickness from a few millimeters to several centimeters. Occasionally, metatexite shows a transition from its typical banded structure to an isotropic equigranular migmatite (diatexite). The migmatites can be separated into three main subtypes according to their bearing mineral assemblages, which are: 1) cordierite-bearing migmatites, 2) cordierite–garnet-bearing migmatites with and without sillimanite and 3) garnet-bearing migmatites. Cordierite-bearing migmatites are restricted to the eastern section mainly associated with the silicic unit, whereas garnet-bearing migmatites appear in the mafic unit, to the west. Cordierite- and garnet-bearing migmatites predominate in the central portion of the Valle Fértil section and also appear subordinate where one of the other subtypes is dominant.

Cordierite-bearing migmatites (specimen GVF53, Fig. 2 and Table 1) exhibit a homogeneous granoblastic dominated texture (Fig. 3a), and mesosome and leucosome are more difficult to distinguish than in the other migmatites. Foliation is defined by the parallel alignment of biotite, with plagioclase and quartz locally elongated parallel to the biotite orientation. Alkali feldspar occur as anhedral grains ranging from 0.65 to 1.20 mm with lobate boundaries. In general, it develops simplectite texture in contact with quartz, with inclusions of biotite, Fe–Ti oxide, and quartz. Quartz occurs as anhedral grains with lobate boundaries and displays undulatory extinction and lamellae. In places, quartz grains have fine grained recrystallized rims. Cordierite occurs as anhedral, medium-sized grains with polysynthetic twins. Cordierite also occurs as subhedral porphyroblasts with quartz, biotite, and oxide inclusions. Plagioclase is present as subhedral crystals of small to medium size with lobate boundaries and display simplectite textures when it is in contact with alkali feldspar. Biotite appears as small to medium reddish flakes with serrate boundary.

Garnet–cordierite-bearing migmatites without sillimanite (specimen GVF54, Fig. 2 and Table 1) have melanosomes with lepidoblastic textures that consist of biotite, plagioclase, cordierite, garnet, quartz, and Fe–Ti oxides. Biotite appears as small, elongated flakes with preferred mineral orientation. In places, biotite forms nearly monomineralic clusters that wrap around garnet. Quartz commonly occurs as lobate or serrate equigranular crystals and in places appears as elongated grains aligned parallel to the metamorphic foliation. Cordierite occurs as porphyroblasts with polysynthetic twinning, and commonly contains aligned inclusion of biotite, Fe–Ti oxides and quartz. Locally, cordierite forms clusters of grains with pseudo-polygonal texture. Garnet occurs as small euhedral or slightly larger subhedral crystals ranging in size from 0.6 to 1.7 mm. Commonly, garnet poikilitically encloses biotite, oxides, and rounded quartz (Fig. 3b). In places, garnet grains are embayed and filled with quartz. Some garnets have ameboidal shapes, resulting from agglomeration of several crystals. Few garnets include several grains of optically continuous cordierite.

Leucosomes are dominated by quartz and plagioclase with or without garnet and have hypidiomorphic granular texture (Fig. 3c). Quartz is fine to medium-grained, occurs as lobate grains, and has undulatory extinction. Plagioclase appears as euhedral grains with

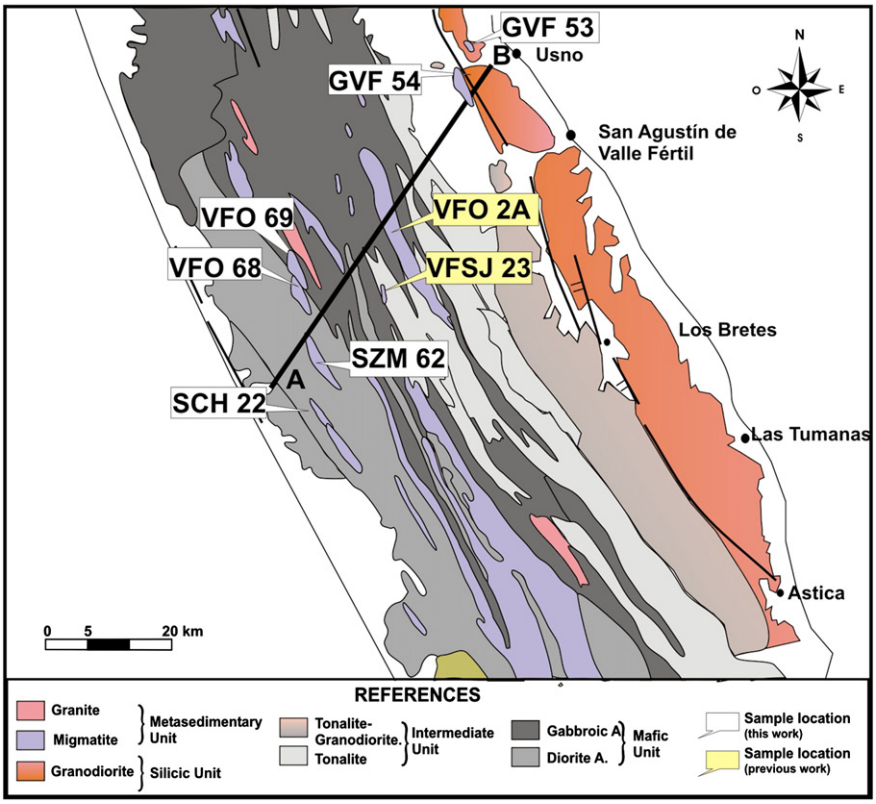

Fig. 2. Simplified geologic map of study area, from the inset of Fig. 1b. Sample locations for this study are shown, along a transverse across the entire range from the deepest to the shallower level. Paleo-up is to the northeast.
Simplified geologic map modified from Mirré (1976), Otamendi et al. (2009) and Vujovich et al. (1996).

Table 1
General characterization and location of migmatites.

Sample	Rock type	Location	Mineralogy
VFG53	*Cordierite bearing migmatite*	67°34′11.1″; 30°34′18″	Qtz–Pl–Crd–Kfs–Bt (Zrc–Op)
VFG54	*Garnet–cordierite bearing migmatite*	67°34′18.2″; 30°34′47″	Qtz–Pl–Bt–Grt–Crd (Op–Spl)
VFO68/69	*Garnet–cordierite–sillimanite bearing migmatite*	67°40′17.7″; 30°42′25.9″	Qtz–Pl–Grt–Bt–Sil–Crd–Kfs (Zrc–Op–Spl)
SZM62	*Garnet bearing migmatite*	67°40′6.6″; 30°46′31.8″	Qtz–Pl–Bt–Sil–Grt (Zrc–Op)
SCH22	*Garnet bearing migmatite*	67°35′46.9″; 30°42′13.7″	Qtz–Pl–Bt–Sil–Grt–Kfs (Zrc–Ap–Op–Mnz)

lobate boundaries. When present, garnet occurs in leucosomes as small, reabsorbed grains. Cordierite appears in very low proportions as isolated grains usually surrounded by quartz.

In *garnet–cordierite–sillimanite-bearing migmatites* (VFO68 and VFO69, Fig. 2 and Table 1) mesosomes form thin granolepidoblastic layers mainly consisting of biotite with subordinate sillimanite and quartz. Biotite occurs as subhedral grains elongated parallel to the mesoscopic foliation. Sillimanite is always texturally associated with biotite and forms subhedral prismatic crystals that occur both as discrete grains and as aggregates (Fig. 3d). Quartz appears as subhedral to anhedral grains with lobate boundaries.

Leucosomes are composed of quartz, plagioclase, K-feldspar, cordierite, and garnet and typically have granoblastic textures. Quartz occurs as small to medium anhedral elongated grains with lobate boundaries. In general, quartz has undulatory extinction and locally is recrystallized to form fine-grained domains. Alkali feldspar is present as anhedral crystals with lobate grain boundaries, and in places is elongated parallel to the foliation. Plagioclase occurs as subhedral laths with polysynthetic twins, sometimes housing inclusion of oxides, biotite, spinel, and quartz. Cordierite appears as subhedral crystals that are usually partly transformed to pinnite. Cordierite also occurs as twinned porphyroblasts poikilitically enclosing biotite, sillimanite, and quartz (Fig. 3f). Garnet appears either as subhedral to euhedral porphyroblasts with reabsorbed rims or as crystals that poikilitically enclose biotite, quartz, and oxides (Fig. 3f). Garnet also appears as inclusion-free crystals with ameboidal shape.

In *garnet-bearing migmatites* (specimens SCH22 and SZM62, Fig. 2 and Table 1) mesosomes consist of biotite, sillimanite, garnet, quartz, plagioclase, and Fe–Ti oxides (Fig. 3g). The foliation is defined by preferred mineral orientations of biotite, plagioclase, elongated quartz,

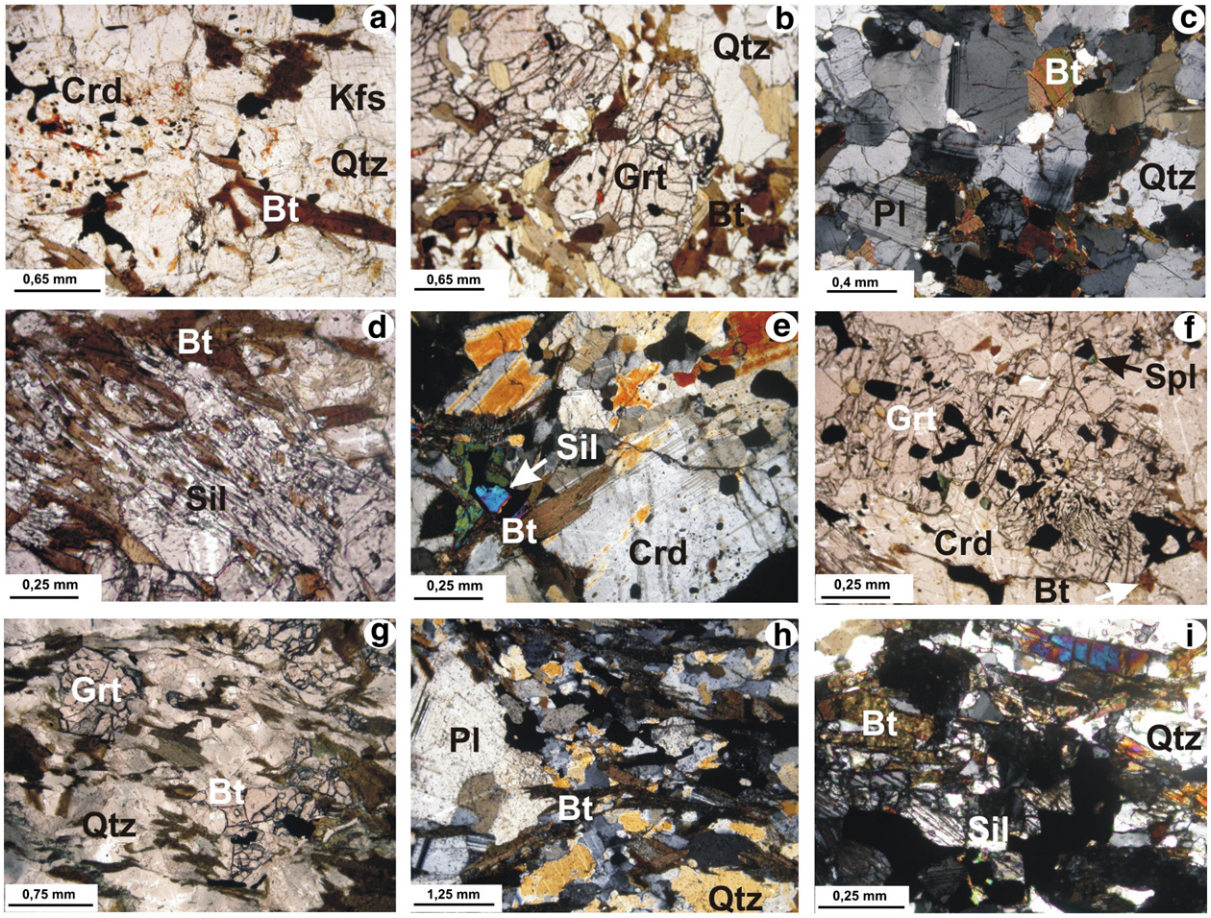

Fig. 3. Photomicrographs of the migmatites from the central part of the Sierra de Valle Fértil. (a) Typical granoblastic texture in cordierite-bearing migmatites (GVF53). (b) Mesocratic domain in garnet–cordierite-bearing migmatite (GVF54) showing the presence of small, euhedral garnet and garnet porphyroblast with poikilitic inclusions of biotite, oxides, and rounded quartz. (c) Leucosomes dominated by fine to medium-grained quartz and euhedral grains of plagioclase, showing equigranoblastic texture in garnet–cordierite-bearing migmatite (GVF54). (d) Coarse-grained aggregate of idioblastic sillimanite intergrown with quartz and biotite in garnet–cordierite–sillimanite-bearing migmatite (VFO68). (e) Clustered grains of idioblastic cordierite within the leucosome of migmatite VFO69. Cordierite also occurs as poikilitic porphyroblasts including several grains of biotite, sillimanite, and quartz. Cordierite is partly pinitized and porphyroblasts commonly show polysynthetic twins. (f) Garnet porphyroblasts with reabsorbed rims that include biotite, quartz, and oxides (VFO68). (g) Typical granolepidoblastic texture in garnet-bearing migmatites, mesosomes consisting of biotite, sillimanite, garnet, quartz, plagioclase, and Fe–Ti oxides. (h) Foliation in garnet-bearing migmatite defined by mineral preferred orientations of biotite, plagioclase, elongated quartz, and prismatic sillimanite. (i) Idioblastic to subidioblastic sillimanite intergrown with quartz and biotite along the foliation planes.
Mineral abbreviations after Kretz (1983).

and prismatic sillimanite (Fig. 3h). Locally, biotite, sillimanite, and quartz show anastomozing foliation around garnet. Sillimanite appears as granoblasts up to 1 mm in length (Fig. 3i), and in places have simplectitic intergrowths with quartz and biotite. Quartz appears as small grains with lobate to serrate boundaries. Garnet occurs as porphyroblasts ranging in size from 0.5 to 1.5 mm, which commonly has inclusions of quartz, biotite, spinel, and Fe–Ti oxides. Garnet also has embayed rims in contact with quartz and/or quartz filled core holes. Spinel always appears as oval inclusions associated to Fe–Ti oxides inside garnet.

The leucosomes are coarser-grained than melanosomes and have granoblastic texture and comprising interlocking quartz, plagioclase, alkali feldspar, and rare biotite with or without garnet. Plagioclase, alkali feldspar, and quartz are the dominant minerals and in general are elongated parallel to the migmatite's foliation. In places, plagioclase occurs as porphyroblasts. Alkali feldspar and quartz occur together as myrmekitic intergrowths.

5. Mineral chemistry

Electron microprobe analyses were conducted at the University of Huelva, Spain using a JEOL JXA-8200 Superprobe equipped with four wavelength dispersive X-ray spectrometers. Two spectrometers are equipped with LIFH and PETH crystals, and the two others combined a distinct set of LIF, PETJ, TAP, LDE1, LDE2 and LDEB crystals. Counting times for each element were between 10s and 30s at an accelerating potential of 15 kV, a beam current of 20 nA and width of around 5 μm. Analyses not obeying the following criteria were discarded: garnets and plagioclases with totals outside the range 100 wt.% ± 1, biotites with totals outside the range 96 wt.% ± 2, and cordierites with total lower than 96.5%. Mineral compositions were further tested using stoichiometric constraints. Operating conditions for X-ray map collection used a 5 μm beam diameter, a beam current of 40 nA and dwell times of 10 ms. Both natural and synthesized materials were used as standards. Representative compositions of metamorphic minerals are presented from Tables A.1 to A.4.

Irrespective of the coexisting mineral assemblages, garnets are solid solutions dominated by almandine and pyrope end members, and exhibit zoning patterns characterized by a wide compositionally uniform core with a narrow zoned rim (Fig. 4). In cordierite–garnet-bearing migmatites, garnet is compositionally homogeneous with slight chemical zoning towards rims of increasing X_{Fe} from 0.61 to 0.63 ($X_{Fe} = Fe^{2+}/Fe^{2+} + Mg + Ca + Mn$, in atoms per unit formula), X_{Mg} from 0.19 to 0.22, and X_{Ca} from 0.03 to 0.04. In contrast, X_{Mn} ratio remains constant at 0.13 throughout the grains (Figs. 4a and 5). Garnet zoning pattern in cordierite–garnet–sillimanite-bearing migmatites also displays a wide compositionally homogeneous core, but is different from that of the sillimanite-absent migmatites in having lower X_{Fe} and X_{Ca} (Fig. 4b). In addition, garnet–cordierite–sillimanite-bearing migmatites contains garnet with the highest pyrope abundances measured as X_{Mg} of about 0.35. The composition of garnets in cordierite-absent garnet-bearing migmatites display little differences with respect to the zoning patterns of garnet in cordierite-bearing migmatites (Fig. 4a to d). In a garnet migmatite (SZM62), garnet porphyroblast has the lowest X_{Mg} combined with the highest X_{Ca}, but the abundances of Fe and Mn are similar to those of cordierite-bearing migmatites (Fig. 4c). The other garnet-bearing migmatite (SCH22) has garnets that are often broken and resorbed, but spessartine (X_{Mn}) enriched rims normally formed after extensive resorption is not observed (e.g., Robinson, 1991; Spear, 1993).

In both garnet migmatites and garnet–cordierite–sillimanite migmatites, biotites have nearly the same composition with X_{Mg} ($X_{Mg} = Mg/Mg + Fe^{2+}$) ranging from 0.56 to 0.62; yet, X_{Mg} of biotites varies less than 0.2 within every single specimen. Most of these biotites also contain high abundances of TiO_2 (3.5–4.8 wt.%),

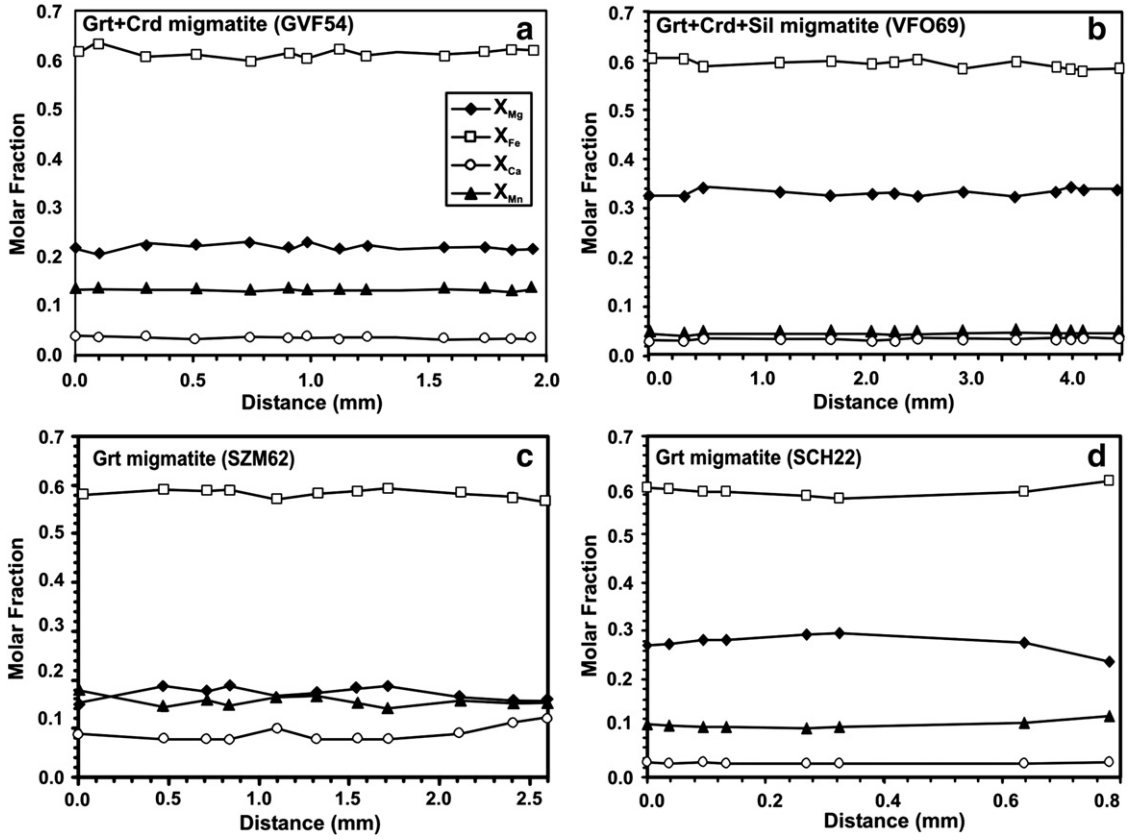

Fig. 4. Chemical profile for garnet porphyroblasts from the different migmatites types recognized in the central part of the Valle Fértil section.

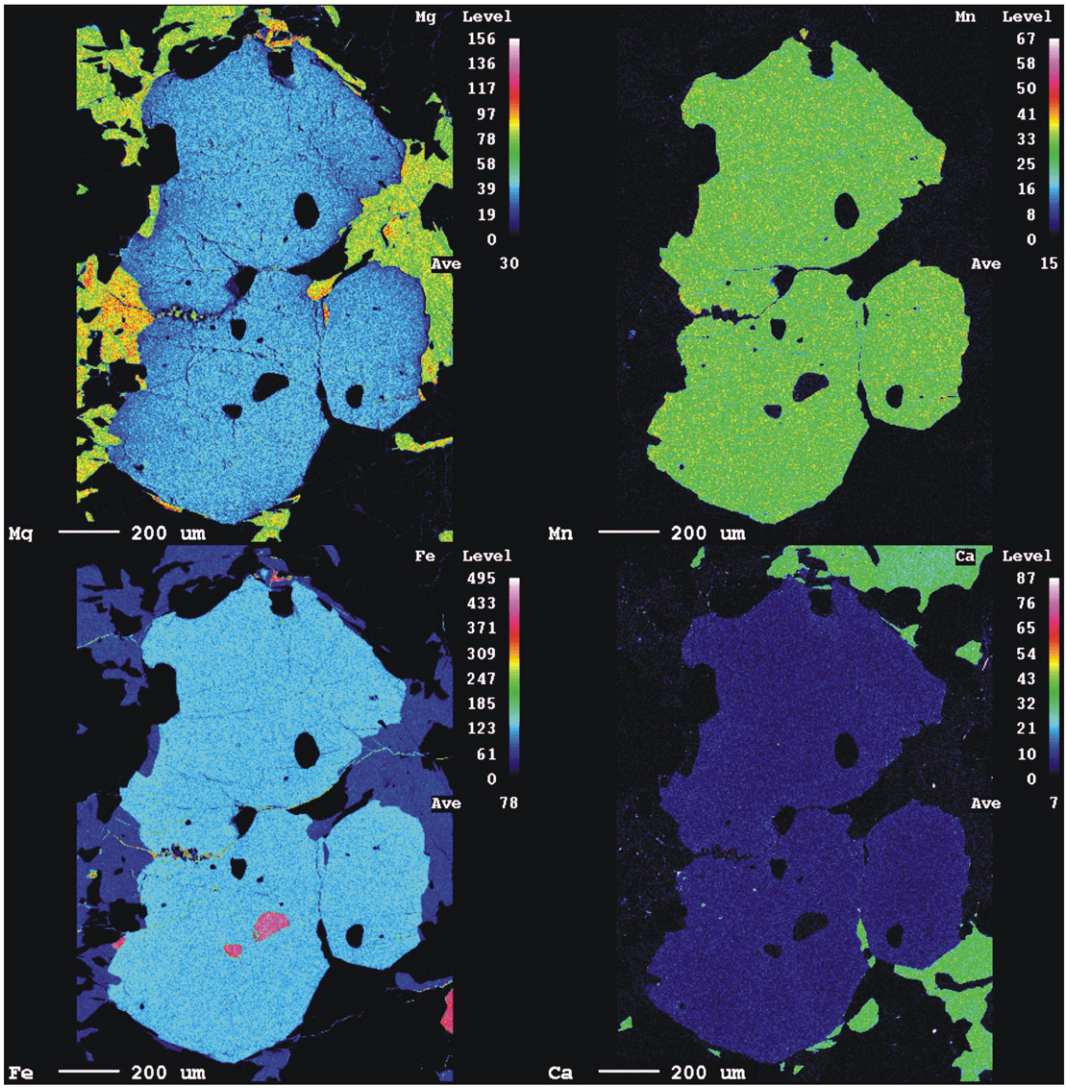

Fig. 5. X-ray compositional maps measured for qualitatively analyzing the 2-D distribution of Fe, Mg, Ca, and Mn on the garnet porphyroblast from garnet–cordierite bearing migmatite.

with the notable exception of biotites in a garnet migmatite (SZM62) that have TiO_2 contents between 2.5 and 3.0 wt.%. Biotites in garnet–cordierite-bearing migmatites have relatively low X_{Mg} between 0.56 and 0.59; however, they show the same compositional features including TiO_2 (2.9–3.4 wt.%.) contents as biotites coexisting with other mineral assemblages. As granulite facies paragneissic migmatites from the Sierra de Valle Fértil possess similar whole rock Mg/Fe ratios and consist of ilmenite-bearing assemblages (Gallien et al., 2010; Otamendi et al., 2008; Tibaldi et al., 2011), numerous biotites display two evidence of retaining their peak temperature compositions, these are: 1 — variation of X_{Mg} over narrow ranges, and 2 — concentration of TiO_2 found to be high (Patiño Douce et al., 1993).

The mineral composition of plagioclase varies depending on the mineral assemblage of its associated rock. Plagioclase from garnet-bearing migmatites is oligoclase (An_{24}–An_{26}). In contrast, plagioclase in garnet–cordierite-bearing (with and without sillimanite) and cordierite bearing migmatites is andesine (An_{30}–An_{46}). When present, alkali feldspar is mesoperthitic with subordinate percentages of albite which varies from 11% to 16%.

Cordierite composition in garnet–cordierite- and cordierite-bearing migmatites is similar with Mg# ranging from 0.73 to 0.76. These cordierites have normal abundance of MnO (0.3–0.5 wt.%) and Na_2O (0.09–0.1 wt.%). Some cordierites from garnet–cordierite-bearing migmatites have high Mg# between 0.77 and 0.84.

Fe–Ti oxides are the unique opaque minerals. In most cases, oxides are magnetites. Ti-bearing oxides have TiO_2 up to 16 wt.%. The latter Fe–Ti oxides are solid solutions with X_{Ilm} (mole fraction of the $FeTiO_3$ phase component) ranging from 0.52 to 0.65.

6. Thermobarometry

6.1. Methodology

To reconstruct the physical and chemical structure of the Valle Fértil arc, we determined the equilibrium pressures and temperatures for metasedimentary packages intercalated with igneous rocks at different structural levels. Chosen samples were collected along a transverse across the entire range from the deepest to the shallower levels exposed in the central part of the Valle Fértil complex (Fig. 2).

Samples SCH22 and SZM62 were taken from the western exposures of the Sierra de Valle Fértil at present-day coordinates 67°35′46.9″ south 30°42′13.7″ west and 67°40′6.6″ south 30°46′31.8″ west, respectively. They are granulite-facies migmatites interbedded with gabbroic and dioritic rocks, and are part of the lowest exposed levels of the

mafic unit from Valle Fértil. Samples VFO68 and VFO69 are also from the central part of Valle Fértil, but collected in Quebrada Otarola. These migmatites make up large lenses interlayered with the diorite and gabbroic rocks at the upper levels of the mafic unit. Sample GVF53 (67°34′11.1″; 30°34′18″) and GVF54 (67°34′18.2″; 30°34′47″) are from a large metasedimentary body within the granodiorite zone, near its eastern border (Fig. 2).

Equilibrium temperatures and pressures were estimated through the following exchange and net transfer reactions:

$$Fe_3Al_2Si_3O_{12} + KMg_3AlSi_3O_{10}(OH)_2 = Mg_3Al_2Si_3O_{12} + KFe_3AlSi_3O_{10}(OH)_2$$
(Fe − Mg/Bt − Grt)
almandine + phlogopite = pyrope + annite

$$Ca_3Al_2Si_3O_{12} + 2Al_2SiO_5 + SiO_2 = 3CaAl_2Si_2O_8 \quad (GASP)$$
grossularite + sillimanite + quartz = anorthite

$$3CaAl_2Si_2O_8 = Al_2(Mg,Fe)_{-3} + Ca_3Al_2Si_3O_{12} + (Mg,Fe)_3Al_2Si_3O_{12} \quad (GBP)$$
anorthite = Al in biotite + grossularite + almandine/pyrope

$$2Fe_3Al_2Si_3O_{12} + 3Mg_2Al_4Si_5O_{18} = 2Mg_3Al_2Si_3O_{12} + 3Fe_2Al_4Si_5O_{18}$$
(Fe − Mg/Crd − Grt)
almandine + Mg−cordierite = pyrope + Fe − cordierite

$$2(Fe,Mg)_3Al_2Si_3O_{12} + 5SiO_2 + 4Al_2SiO_5 + 3nH_2O = 3(Fe,Mg)_2Al_4Si_5O_{18}.nH_2O(CGQS)$$
almandine/pyrope + quartz + sillimanite + water = Fe − cordierite/Mg − cordierite

Temperature and pressure determinations were calculated using both: i) the thermodynamic standard state properties of Berman (1988) and Berman and Aranovich (1996), using the no ideal solid solutions model of Berman (1990) for garnet, Holland and Powell (1992) for plagioclase, Patiño Douce et al. (1993) for biotite, Berman and Aranovich (1996) for cordierite; and ii) the (TH) Thermocalc database of Holland and Powell (1998). In this case, activities were calculated using the program AX by T. Holland.

6.2. P–T determinations

One of the critical limitations to estimate P–T conditions in granulite facies metamorphism is that reactions involving Fe–Mg exchange are affected by retrogression upon cooling (Kohn a Spear, 2000; Pattison et al., 2003; Spear, 1993). In order to minimize this phenomenon and remove their effect it is crucial to establish the chemical variations in mineral phases. Spear (1993) showed that peak metamorphic temperatures from biotite–garnet Fe–Mg exchange thermometry may be tenable in granulite facies rocks provided that the garnet composition was homogenized at the peak temperature and remain unmodified during cooling. The peak composition of garnet would be better preserved when: 1 — garnet grew as crystals with radii larger than 1 mm, 2 — the modal abundance of garnet was always lower than that of biotite, and 3 — the rock experienced retrograde evolution dominated by a high cooling rate. Migmatites selected for this study have garnet porphyroblasts (>1 mm) with nearly homogeneous compositional zoning and mineral assemblages where the modal proportion of biotite is always higher than that of garnet. Simple textural relations and constant mineral compositions make easy the interpretation of geothermobarometric results. However, in order to evaluate the possibility of resetting by Fe–Mg ion-exchange between garnet and biotite, P–T calculations were performed using core and rim garnet composition combined with biotites located in the matrix or in direct contact with garnet (e.g., Spear, 1993).

Equilibrium temperature estimates in sample SCH22, using either core and rim compositions indicate that the garnet-bearing migmatite studied at the base of the arc section equilibrated at temperatures ranging from 850 to 900 °C and pressures of 8.3 ± 1.1 kbar (GASP), 8.25 ± 1.0 kbar (GBP), and 8.3 ± 1.7 kbar (TH) (Table 2 and Fig. 6). The agreement of barometric estimates through two thermodynamic databases, with distinct heat capacity parameters, compressibility coefficients and equations indicates that the P–T condition calculations from the base of the paleoarc are independent of the P–T approach.

In sample SZM62, P–T estimates are similar to those achieved in the western most exposed levels (SCH22); however, more variable results are observed when rim against core compositions are used. Temperature calculations using Fe–Mg exchange in Grt–Bt with both Berman's database and the Thermocalc algorithm range between 730 and 850 °C for core compositions, whereas temperatures from 720 to 800 °C are obtained when rim compositions are used. Pressure determinations in this lithology are also more variable depending on the barometer (see Table 2 and Fig. 6). The GASP barometer estimates reveal higher pressures (8.5 ± 1.0 kbar) than those achieved with the GOP barometer (8.0 ± 1.3 kbar) and with TH (7.3 ± 1.1 kbar). However, despite these differences, equilibrium pressure estimates all fall around 8.0 ± 1.0 kbar (Table 2 and Fig. 6).

Table 2
P–T estimations for the Valle Fértil migmatite rocks.

Sample	Method	T, °C	Method	T, °C	Method[g]	P, kbar	Method[g]	P, kbar	Method	T, °C	P, kbar	Method	T, °C	P, kbar
GVF54[a]	GB[c]	738 ± 35	GC[c]	700 ± 45	GASP	5.3 ± 1.1	GBP	6.2 ± 1.3	TH(gbps)	731 ± 138	5.5 ± 1.5	TH(gbpsc)	756 ± 61	5.0 ± 0.9
GVF54[b]	GB[c]	676 ± 20	GC[c]	689 ± 63	GASP	5.2 ± 1.0	GBP	6.0 ± 1.1	TH(gbps)	686 ± 143	6.5 ± 1.4	TH(gbpsc)	655 ± 79	5.1 ± 0.8
VFO68[a]	GB[d]	895 ± 25	GC[d]	720 ± 25	GASP	7.0 ± 1.0	GBP	8.0 ± 1.1	TH(gbps)	990 ± 155	7.3 ± 1.6	TH(gbpsc)	864 ± 61	7.4 ± 0.8
VFO68[b]	GB[d]	860 ± 30	GC[d]	676 ± 70	GASP	6.8 ± 0.9	GBP	7.5 ± 1.2	TH(gbps)	950 ± 110	6.7 ± 1.4	TH(gbpsc)	862 ± 61	7.3 ± 0.8
VFO69[a]	GB[d]	895 ± 28	GC[d]	714 ± 64	GASP	7.5 ± 1.2	GBP	8.2 ± 1.2	TH(gbps)	910 ± 95	7.1 ± 1.6	TH(gbpsc)	873 ± 56	7.1 ± 0.8
VFO69[b]	GB[d]	855 ± 34	GC[d]	680 ± 76	GASP	6.9 ± 1.4	GBP	7.0 ± 1.6	TH(gbps)	888 ± 150	6.7 ± 1.6	TH(gbpsc)	865 ± 55	7.0 ± 0.8
SZM62[a]	GB[e]	850 ± 100	GC[e]	–	GASP	8.5 ± 1.0	GBP	8.0 ± 1.3	TH(gbps)	728 ± 79	7.8 ± 2.0	TH(gbpsc)	–	–
SZM62[b]	GB[e]	800 ± 130	GC[e]	–	GASP	8.0 ± 1.2	GBP	7.5 ± 1.4	TH(gbps)	720 ± 165	7.3 ± 1.1	TH(gbpsc)	–	–
SCH22[a]	GB[f]	876 ± 11	GC[f]	–	GASP	8.3 ± 1.0	GBP	8.3 ± 1.0	TH(gbps)	900 ± 260	8.4 ± 1.4	TH(gbpsc)	–	–
SCH22[b]	GB[f]	850 ± 33	GC[f]	–	GASP	8.2 ± 1.1	GBP	8.2 ± 1.0	TH(gbps)	846 ± 115	8.2 ± 1.7	TH(gbpsc)	–	–

T–P calculations are: (°C ± 1σ) and (kbar ± 1σ) respectively. Ion-exchange and net-transfer reactions with thermometric and barometric properties from Berman (1988) and Berman and Aranovich (1996) are: (GB), Alm + Py = Phl + Ann; (GC), 2Alm + 3 Mg–Crd = 2Py + 3Fe–Crd; (GASP), Grt + Sil + Qtz = Pl; (GBP), (Al_2Fe_{-3}/Al_2Mg_{-3})Bt + Grs + Alm/Prp = 3An. When using Berman (1988) and Berman and Aranovich (1996) databases, T and P uncertainties (1σ) are obtained computing more than a dozen of compositional data in every sample. Thermobarometric estimations using Thermocalc (TH) with (gbps) and (gbpsc) equilibria involving: g, garnet; b, biotite; p, plagioclase; s, sillimanite; c, cordierite.

[a] Core mineral composition.
[b] Rim mineral composition.
[c] T calculation for 4 kbar.
[d] T calculation for 7 kbar.
[e] T calculation for 8 kbar.
[f] T calculation for 8.3 kbar.
[g] Pressure calculations at T corresponding to GB thermometer.

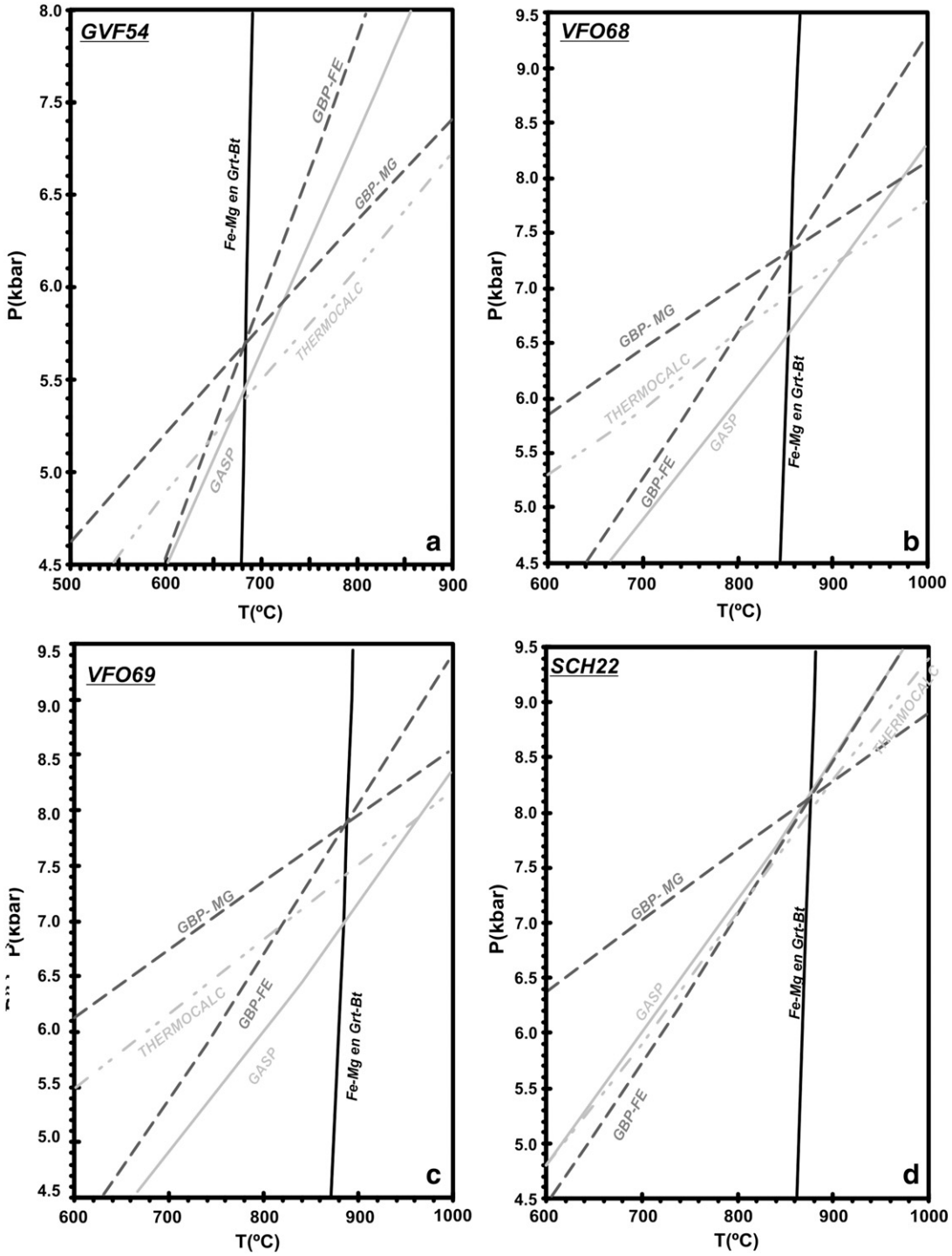

Fig. 6. a–d) Equilibrium calculations for garnet–cordierite-, garnet–cordierite–sillimanite- and garnet-bearing migmatites using core compositions of uniform and zoned plagioclase. Biotite–garnet Fe–Mg exchange, GASP and GBP barometer were computed with the Berman (1988) and Berman and Aranovich (1996) database. Thermocalc mode 2 average pressure calculations (Holland and Powell, 1998).

In the Quebrada Otarola thermometric calculation using the Fe–Mg exchange vector between Grt and Bt indicates that these rocks equilibrated at 850–895 °C (Berman, 1988) and 880–900 °C (TH). This range of values coincides with the TH estimate calculated for the garnet–cordierite pairs (880 ± 65 °C), although the temperatures are systematically higher than estimations obtain with Berman's database (710 ± 25 °C). The GASP barometer yields a pressure estimate of 6.8–7.6 kbar, whereas GBP barometry yields pressures of 7.0–8.0 kbar. Using Thermocalc, multi-reaction equilibria that involve Grt + Bt + Pl + Qtz ± Sil with and without Crd converge at pressures of 7.3 ± 1.5 kbar. These pressures are in the same range as the pressure (6.9–7.1 kbar) obtained with the database of Berman (1988). Taking all of these methods into account suggests equilibration conditions at 870 ± 20 °C and 7.3 ± 1.0 kbar for the Otarola migmatites (Table 2 and Fig. 6). These values are consistent, although slightly higher than the estimates presented in Otamendi et al. (2008) from migmatites (VFO2 in Fig. 2) that are 10 km toward the east in the vicinity of the intermediate unit. The P–T equilibration values are also higher than P–T estimates retrieved from migmatites collected at the transitional/mafic unit boundary (e.g. Tibaldi et al., 2009, 2011).

A sillimanite-free, garnet–cordierite bearing migmatite (sample GVF54) from a metasedimentary block in the silicic unit yields P–T values that correspond to the shallowest paleodepth in the Valle Fértil section. Equilibrium temperatures calculated with Grt–Bt thermometry and the Berman database of 676 and 738 °C for core and rim compositions. Temperatures in the same range (686–731 °C) are obtained with TH for Grt–Bt and Crd–Grt thermometry. There are not significant differences between calculated temperatures involving rim vs. core compositions. Pressure estimates from the GBP barometer indicate this rock equilibrated at 6.2 ± 1.0 kbar, whereas GASP yields a pressure of 5.3 kbar. Because the mineral assemblage lacks sillimanite, GASP determinations should be considered as a maximum pressure estimate. Thermocalc multi-equilibria reaction involving Grt + Bt + Pl + Qtz yields a pressure of 5.5 ± 1.5 kbar, which is within the range of the estimates using the Berman's database (Table 2 and Fig. 6). Similarly, when cordierite is included into the Thermocalc runs, the average values of pressure converge to 5.0 kbar without significant differences.

7. Discussion

7.1. Geological reconstruction of the Valle Fértil paleo-arc

Geothermobarometric estimates yield the depths where metasedimentary rocks experienced peak metamorphic temperatures (Table 2). Since metasedimentary rocks are screens interspersed with igneous plutonic rocks throughout the Valle Fértil section, estimated pressures of thermal peak mineral assemblages allow us to reconstruct the crustal structure. The approach combines barometric estimates from metasedimentary rocks with physical properties calculated using mineral chemistry from the plutonic rocks that dominate the distinct litho-stratigraphic units in a continuous crustal section.

In general, peak metamorphic pressures are converted to corresponding paleodepth. While an often-used method for constraining the internal structure of ancient crustal sections is to calculate seismic wave velocities as a function of paleodepths, and then compare the profile of seismic velocities with geophysical data and models (Behn and Kelemen, 2006; Calvert, 2011; DeBari and Greene, 2011; Hacker et al., 2008; Miller and Christensen, 1994; Sobolev and Babeyko, 2004). For the case of ancient crustal sections, exposed rocks are utilized to estimate P and S wave velocities using thermodynamic parameters and equations to compute their physical properties at the P–T conditions where they once resided. Here, we use the third order finite strain theory developed by Hacker and Abers (2004). Additionally, in order to consider the diversity of rocks observed in the different units, we used a weighting factor over the velocities estimation base on geological mapping that provide 2-D relative proportions of plutonic rock types within a given lithologic unit.

Since the lowest pressure estimated at Valle Fértil section is of 5 ± 1.0 kbar, the overlying crustal column has to be restored from what has been observed in the upper crust of the Famatinian arc north of the Valle Fértil section (Astini, 1998; Astini and Dávila, 2004; Clemens and Miller, 1996; Collo et al., 2009; Mángano and Buatois, 2004;

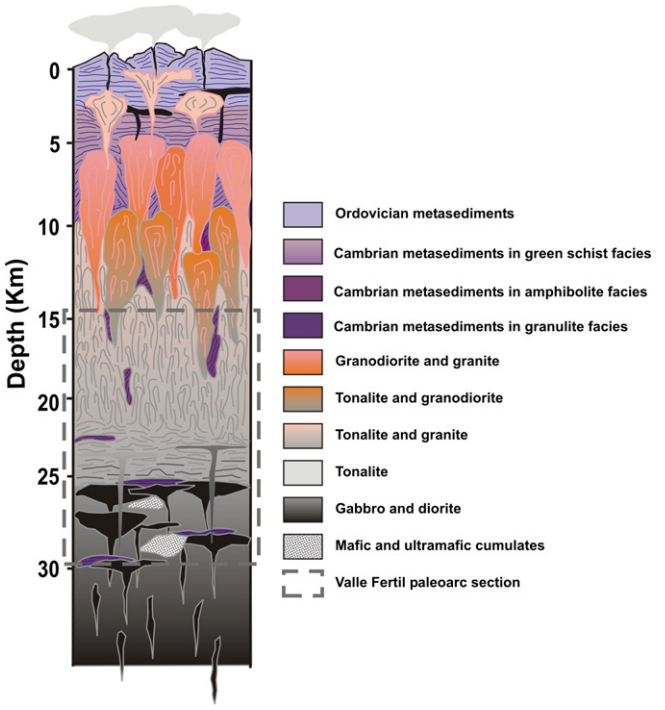

Fig. 8. Reconstructed column for the central part of Sierra de Valle Fértil on the basis of thermobarometry data from metasedimentary rocks interspersed at different levels with igneous plutonic rocks.
The model of batholithic structure takes the main features outlined by the work of Saleeby et al. (2003).

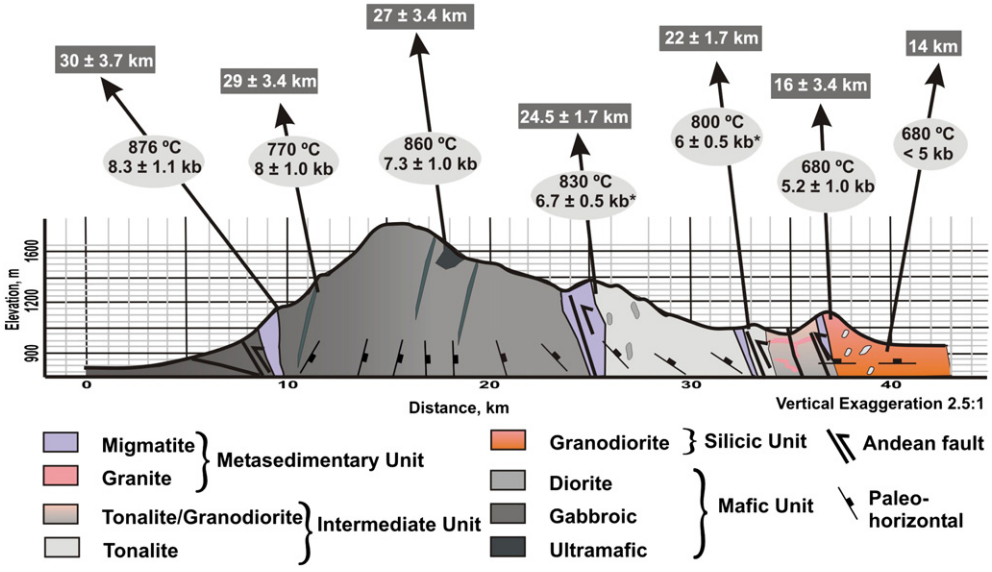

Fig. 7. Cross-section through the central part of the Sierra of Valle Fértil showing P–T conditions and estimated depths.
*Data taken from Otamendi et al. (2008) and Tibaldi et al. (2011).

Table 3
Calculated seismic velocities, mineral proportion and compositions of the different lithological types from the lithostratigraphic units recognized in the Valle Fértil section.

Sample	VFJA 7	VFO 8	VFO 6/1A	VFO 1a	VFO 9	VFJA 6	VFJA 4	SCH 22	SZM 62	VFO 68/69	VFKS 5	VFMJ 14	VFMJ 34A	GVF 12	VFMJ 40B/D	GVF 30	GVF 31	GVF 54
Rock type	Ol–Gb	Amph–Gb	Dio	Dio		Ol–Amph Gb	Amph–Cpx Gb	Mig	Mig	Mig	Dio	Ton	Ton	Gd	Grt			
Unit	MU	MU	MU	MU	MU	MU	MU	MU	MU	MU	IU	IU	SU	SU	SU	SU	SU	SU
Modal proportions																		
Qtz %vol			19.00	23.00	5.15			50.62	31.41	50.81	10.00	25.00	28.00	35.00	36.00	28.00	18.00	49.87
Pl %vol	21.00	37.00	51.00	42.00	40.21	12.00	42.00	20.57	35.68	19.96	57.00	44.00	41.00	34.00	14.00	41.00	47.00	13.72
Kfs %vol	–	–	–	–	–	–	–	4.29	1.65	2.32	–	–	–	12.00	46.00	3.00	–	1.35
Grt %vol	–	–	–	–	–	–	–	3.06	1.92	9.21	–	–	–	–	–	–		11.15
Ol %vol	9.00	–	–	–	–	40.00	–	–	–	0.00	–	–	–	–	–	–	–	–
Opx %vol	11.00	11.00	6.00	–	2.06	12.00	17.00	–	–	0.00	–	–	–	–	–	–	–	–
Cpx %vol	9.00	–	–	–	1.03	1.00	15.00	–	–	0.00	–	–	–	–	–	–	–	–
Amph %vol	40.00	49.00	14.00	19.00	47.42	25.00	23.00	–	–	0.00	20.00	–	7.00	4.00	–	10.00	14.00	–
Bt %vol	–	–	6.00	14.00	–	–	–	20.64	27.02	15.09	10.00	27.00	20.00	10.00	3.00	16.00	16.00	22.77
Ep %vol	–	–	–	–	–	–	–	–	–	0.00	–	1.00	1.00	3.00		1.00	1.00	–
Sil %vol	–	–	–	–	–	–	–	0.20	0.75	1.01		–	–	–	–	–	–	–
Spl %vol	7.00	–	–	–	–	7.00	–	–	–	0.00	–	–	–	–	–	–	–	–
Mt %vol	3.00	3.00	4.00	2.00	4.12	3.00	3.00	0.60	1.58	1.59	3.00	3.00	3.00	2.00	1.00	1.00	1.00	1.15
Mineral composition																		
An	0.95	0.85	0.70	0.60	0.89	0.95	0.90	0.29	0.46	0.36	0.54	0.45	0.50	0.38	0.23	0.45	0.51	0.32
Ab	0.05	0.15	0.30	0.40	0.11	0.05	0.10	0.71	0.54	0.64	0.46	0.55	0.51	0.62	0.77	0.53	0.49	0.68
Or	–	–	–	–	–	–	–	–	–	0.86	–	–	–	0.85	0.89	0.22	–	0.86
Ab	–	–	–	–	–	–	–	–	–	0.14	–	–	–	0.15	0.11	0.78	–	0.14
Alm	–	–	–	–	–	–	–	0.59	0.59	0.56	–	–	–	–	–	–	–	0.62
Grs	–	–	–	–	–	–	–	0.03	0.08	0.04	–	–	–	–	–	–	–	0.03
Py	–	–	–	–	–	–	–	0.38	0.34	0.41	–	–	–	–	–	–	–	0.22
Fo	0.81	–	–	–	–	0.81	–	–	–	–	–	–	–	–	–	–	–	–
Fa	0.19	–	–	–	–	0.19	–	–	–	–	–	–	–	–	–	–	–	–
En	0.81	0.71	0.65	–	0.70	0.71	0.70	–	–	–	–	–	–	–	–	–	–	–
Fs	0.19	0.29	0.35	–	0.30	0.28	0.30	–	–	–	–	–	–	–	–	–	–	–

Di	0.88	–	–	–	–	0.46	0.47	–	–	–	–	–	–	–	–	–	–	–
Hed	0.12	–	–	–	–	0.45	0.44	–	–	–	–	–	–	–	–	–	–	–
Hb	1.00	1.00	1.00	1.00	1.00	1.00	1.00	–	–	–	1.00	–	1.00	1.00	–	1.00	1.00	–
Bt	–	–	–	–	–	–	–	–	–	–	–	–	–	–	–	–	–	–
Phl	–	–	0.56	0.63	–	–	–	0.54	0.49	0.55	0.57	0.38	0.39	0.37	0.38	0.41	0.45	0.41
Ann	–	–	0.29	0.30	–	–	–	0.37	0.39	0.34	0.28	0.37	0.39	0.38	0.33	0.36	0.43	0.29
Mu	–	–	0.15	0.07	–	–	–	0.09	0.13	0.11	0.15	0.25	0.22	0.25	0.29	0.13	0.11	0.20
Spl	0.55	–	–	–	–	0.56	–	–	–	–	–	–	–	–	–	–	–	–
Herc	0.45	–	–	–	–	0.44	–	–	–	–	–	–	–	–	–	–	–	–
Vp and Vs velocities (km/s)																		
Vp (670 °C, 4.5 kbar)	7.20	6.87	6.35	6.13	6.78	7.42	6.93	5.75	5.78	5.98	6.27	5.80	5.93	5.98	5.92	6.00	6.08	5.88
Vs (670 °C, 4.5 kbar)	4.01	3.79	3.59	3.49	3.76	4.16	3.81	3.47	3.33	3.61	3.46	3.29	3.40	3.48	3.46	3.44	3.41	3.56
Vp (730 °C, 5.5 kbar)	7.18	6.85	6.34	6.13	6.77	7.40	6.91	5.74	5.78	5.97	6.26	5.79	5.92	5.97	5.92	5.99	6.07	5.87
Vs (730 °C, 5.5 kbar)	4.00	3.78	3.58	3.48	3.75	4.14	3.80	3.45	3.31	3.59	3.45	3.28	3.38	3.46	3.44	3.43	3.40	3.54
Vp (800 °C, 6.0 kbar)	7.15	6.83	6.32	6.11	6.75	7.37	6.89	5.72	5.75	5.95	6.24	5.77	5.90	5.95	5.90	5.97	6.05	5.85
Vs (800 °C, 6.0 kbar)	3.98	3.77	3.56	3.46	3.73	4.12	3.78	3.43	3.29	3.57	3.43	3.25	3.36	3.44	3.43	3.41	3.38	3.51
Vp (800 °C, 6.5 kbar)	7.16	6.84	6.33	6.11	6.76	7.38	6.90	5.73	5.76	5.96	6.25	5.78	5.91	5.96	5.91	5.98	6.06	5.86
Vs (800 °C, 6.5 kbar)	3.98	3.77	3.56	3.46	3.74	4.12	3.79	3.43	3.30	3.57	3.44	3.26	3.37	3.44	343	3.41	3.39	3.52
Vp (830 °C, 6.7 kbar)	7.15	6.83	6.32	6.11	6.75	7.36	6.89	5.72	5.76	5.95	6.24	5.77	5.90	5.96	5.91	5.97	6.05	5.85
Vs (830 °C, 6.7 kbar)	3.98	3.77	3.57	3.46	3.74	4.12	3.79	3.43	3.30	3.57	3.44	3.26	3.37	3.45	3.43	3.41	3.39	3.52
Vp (800 °C, 7.0 kbar)	7.16	6.84	6.34	6.12	6.77	7.38	6.90	5.74	5.78	5.97	6.26	5.79	5.92	5.97	5.92	5.99	6.07	5.87
Vs (800 °C, 7.0 kbar)	3.98	3.77	3.57	3.46	3.74	4.12	3.79	3.43	3.30	3.57	3.44	3.26	3.37	3.45	3.43	3.41	3.39	3.52
Vp (800 °C, 7.5 kbar)	7.17	6.85	6.35	6.13	6.77	7.39	6.91	5.75	5.79	5.98	6.27	5.80	5.93	5.98	5.93	6.00	6.08	5.88
Vs (800 °C, 7.5 kbar)	3.98	3.78	3.57	3.47	3.75	4.13	3.80	3.43	3.30	3.57	3.45	3.27	3.37	3.45	3.43	3.42	3.40	3.52
Vp (800 °C, 8.0 kbar)	7.18	6.86	6.36	6.14	6.78	7.39	6.92	5.76	5.80	5.99	6.28	5.81	5.94	5.99	5.94	6.01	6.09	5.88
Vs (800 °C, 8.0 kbar)	3.99	3.78	3.58	3.47	3.75	4.13	3.80	3.43	3.31	3.57	3.45	3.27	3.38	3.46	3.43	3.42	3.40	3.52
Vp (800 °C, 8.5 kbar)	7.18	6.86	6.37	6.15	6.79	7.40	6.93	5.76	5.80	5.99	6.29	5.82	5.95	6.00	5.94	6.02	6.10	5.89
Vs (800 °C, 8.5 kbar)	3.99	3.79	3.58	3.48	3.75	4.13	3.80	3.43	3.31	3.57	3.46	3.27	3.38	3.46	3.44	3.43	3.41	3.52
Vp (870 °C, 8.5 kbar)	7.15	6.84	6.34	6.12	6.76	7.36	6.90	5.73	5.77	5.97	6.25	5.79	5.92	5.97	5.92	5.99	6.07	5.86
Vs (870 °C, 8.5 kbar)	3.97	3.76	3.56	3.45	3.73	4.11	3.78	3.41	3.28	3.55	3.44	3.25	3.36	3.43	3.42	3.40	3.38	3.50
Vp (870 °C, 8.3 kbar)	7.15	6.83	6.33	6.12	6.76	7.36	6.89	5.73	5.77	5.96	6.25	5.78	5.92	5.97	5.92	5.98	6.07	5.86
Vs (870 °C, 8.3 kbar)	3.97	3.76	3.56	3.45	3.73	4.11	3.78	3.41	3.28	3.55	3.43	3.25	3.36	3.43	3.42	3.40	3.38	3.50

Mángano et al., 2003; Mannheim and Miller, 1996; among others). The first 3 km of stratigraphy comprise sedimentary successions deposited from the uppermost Cambrian to the Lower Ordovician, with lavas and volcaniclastic sediments interbedded with the youngest strata (Mángano et al., 2003). Thick quartz-rich turbiditic successions are found below an unconformity near the Cambrian–Ordovician boundary. This unconformity was caused by a tectonic episode that folded, stacked and buried the middle to late Cambrian sedimentary successions to depths of up to 16 km (Collo and Astini, 2008; Cristofolini et al., 2012). However, flat roofs of Early Ordovician batholiths are observed beneath late Cambrian turbiditic successions at 2.5 kbar (Collo and Astini, 2008). From this geological evidence, we assume two layers; the upper layer is a 3-km-thick Early Ordovician sequence with densities of 2.55 to 2.60 g/cm^3 and the underlying layer consist of late Cambrian metasedimentary successions and plutonic granitoids with densities between 2.70 and 2.75 g/cm^3. This assumption yields minimum crystallization depths of about 16 km (4.5 kbar) for the uppermost levels of the silicic unit exposed in the central section of the Sierra de Valle Fértil (Figs. 7 and 8).

The silicic unit composed of a mixture of granodiorites, tonalites and leucogranites emplaced from 16 to 18 km paleodepths with ambient temperatures of 700 ± 30 °C, as suggested by thermometry of metasedimentary screens (Table 2), would have had P wave velocities ranging from 5.9 to 6.1 km/s (Table 3), while the arc was active. The transitional boundary zone separating the silicic from the underlying intermediate unit is made up by the same lithologic types as the silicic unit, but with a preponderance of tonalites. Barometric estimates indicate that this transitional unit extended to depth of 22 km, and the ambient temperature was about 800 °C, hence the complex mixture of plutonic rocks would have yield P wave velocities of 6.2 ± 0.1 km/s.

As currently exposed, the typical intermediate unit is flanked by metasedimentary screens indicating that its thickness encompasses ~0.7 kbar, corresponding to a paleovertical extension of about 3 km. Our thermometric results suggest relatively high ambient temperatures of 810 ± 20 °C. Under these conditions the complex mixture of diorites and tonalites yield P-wave velocities ranging between 6.2 to 6.4 km/s. However, the intermediate unit includes a significant amount of amphibole-rich gabbroic rock entrained as inclusion or intruded as sill/dike tabular bodies (Otamendi et al., 2009). The heterogeneous lithologic nature of the intermediate unit makes it difficult to determine the proportion of the gabbroic component within the unit. However, because a typical amphibole gabbroic rock gives a Vp of 6.8 km/s, which is on average 0.4 km/s higher than those estimated in diorites and tonalites, the existence of 25% of gabbroic component into the dioritic and tonalitic mixture would lead to increase computed P-wave velocities by 0.1 km/s (Fig. 9a).

Importantly, beyond geological problems and thermodynamic extrapolations that are inherent to the procedure of retrieving physical properties at high P–T conditions, Vps inferred for the arc crustal column dominated by quartz–plagioclase–feldspar plutonic rocks are consistent with measured seismic wave velocities for these type of rocks in both laboratory and natural experiments (e.g. Calvert, 2011; Christensen and Mooney, 1995; Fliedner and Klemperer, 2000; Kitamura et al., 2003).

At the deepest exposed paleodepths, the mafic unit is dominated by amphibole-bearing gabbronorites and quartz-poor diorites. Two lithologic types with high densities occur as relatively small bodies but are widespread in the mafic unit: 1) modally layered mafic/ultramafic cumulate rocks; and 2) amphibole gabbro sills and dikes with massive and fine-grained fabrics. The difference in barometric estimates along the mafic unit corresponds to about a 5-km-thick crustal section, and below a paleodepth of 25 km. At pressures above 6.5 kbar, all these lithologies have high seismic wave velocities, with Vp increasing from 6.8 km/s for diorites through 7.0 km/s for amphibole gabbronorites to 7.4 km/s for olivine-bearing gabbroic cumulates. As discussed below, the original lithologic heterogeneity of the mafic unit is even further complicated by extensive tectonic overprinting; however, together the mafic rock types yield P-wave velocities ranging from 6.9 to 7.2 that are typical of lower crustal levels in both continental and oceanic active arcs (Calvert, 2011; Parsons et al., 1998).

The current outcrop width of 30 km of the Valle Fértil plutonic complex exposes ~17 km thickness of the original arc middle crust (Fig. 7), this raises the question of how and when the section was thickened. The discrepancy between present-day and reconstructed paleoarc crustal thickness may arise from uncertainties in the estimated peak metamorphic pressures. The accuracy of even the best calibrated barometers is on the order of ± 230 to ± 890 bars (e.g., Spear, 1993). Thus, the resolution of computed paleodepths may spread over a range of up to ± 3 km. Another cause for this discrepancy may be related to the tectonic reorganization of the Valle Fértil crustal section during the collision with the Cuyania microplate (Astini and Dávila, 2004; Casquet et al., 2001; Castro de Machuca et al., 2007; Comínguez and Ramos, 1991; Ducea et al., 2010; Mulcahy et al., 2011; Otamendi et al., 2008). The late Ordovician to Silurian deformation along the western border of the Valle Fértil section occurs as wide shear zone with E–W convergence and top-to-W stacking (Castro de Machuca et al., 2007; Cristofolini et al., 2010). Collision-related tectonic convergence is likely responsible for the observed thickening, and our fieldwork suggests that it largely repeated crustal slices within the westernmost mafic unit (also see Fig. 2).

7.2. Comparison with ancient and active arcs sections

Two features observed in the Famatinian paleoarc are characteristic of arc crust: 1) a stratified, progressively denser crust with depth, and 2) inflections in Vp with depth. These characteristics contrast with the profile of average continental crust, which is vertically smooth with a mean P-wave velocity of 6.45 km/s between 5 and 50 km depths (Christensen and Mooney, 1995). In most arcs, the uppermost sedimentary and volcaniclastic successions are commonly overlying a well-defined layer with low P-wave seismic velocities between 6.0 and 6.5 km/s (Fig. 9b; Christensen and Mooney, 1995; Kitamura et al., 2003). This low velocity layer, consistent with a bulk composition between granite and tonalite, has been observed, with varying thickness, in both oceanic and continental settings (Calvert, 2011; DeBari and Greene, 2011). In active oceanic arcs such as Kuriles, Izu-Bonin and Mariana the layer with Vp between 6.0 and 6.5 km/s is less than 10 km thick and located at shallow depths ranging from 3 to 14 km (Calvert et al., 2008; Nakanishi et al., 2009; Suyehiro et al., 1996). The active Aleutian destructive margin is unique as it is laterally transitional from oceanic to continental arc crust (e.g. Fliedner and Klemperer, 2000). Despite a marked lateral change in the seismic structure from the oceanic Aleutian to the continental Alaskan arc, there is an absence of a relatively low P-wave velocity middle crustal layer beneath the active volcanic front (Fliedner and Klemperer, 2000). One of the thickest middle crustal low Vp layers in an active arc setting has been found in the Cascadia arc (Parsons et al., 1998) where it is interpreted to be silicic plutons with variable across-arc thickness (<8 km).

The crustal section that we observe at the Famatinian arc, including the assumed upper crustal component, has a low velocity layer extending down to ~22 km paleodepth. This low velocity layer is of similar thickness, though extends deeper, than that measured at the Cascadia arc. Notably, within the Famatinian arc the rocks are directly observed over large exposures, and hence the lower–middle crust inferred to have Vp<6.5 km/s is composed of igneous plutonic rocks ranging from granites to tonalites, consistent with laboratory measurements supported by surface field mapping in the mid crustal Tanzawa plutonic complex from the oceanic Izu arc (Kawate and Arima, 1998; Kitamura et al., 2003).

The change of the dominant lithology from quartz–plagioclase bearing tonalites to amphibole–plagioclase bearing gabbroic rocks at paleodepths between 22 and 25 km results in a prominent increase of computed P wave seismic velocities (Fig. 9b). This feature makes

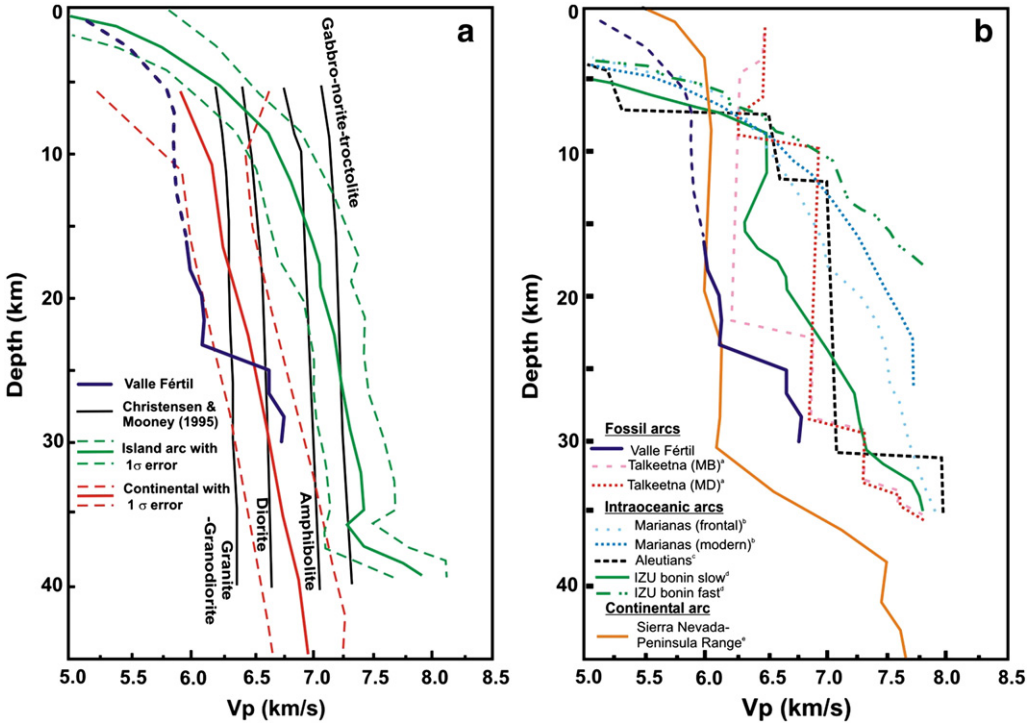

Fig. 9. (a) Comparison of calculated velocity profiles from the central section of the Sierra de Valle Fértil with seismic wave velocities for continental rock types of Christensen and Mooney (1995) and range of velocity values for island arc and continental crust (Christensen and Mooney, 1995). (b) Comparison of calculated velocity profiles from the Sierra de Valle Fértil with those of Talkeetna section and from intraoceanic and continental arcs.
[a]Models B and D of Rioux et al. (2010), [b]Calvert et al. (2008), [c]Holbrook et al. (1999), [d]Kodaira et al. (2007) and [e]Fliedner et al. (2000).

the profile of Vp against depth inferred for the Valle Fértil section to resemble seismic structures measured in the Sierra Nevada arc and reconstructed for Talkeetna paleoarc (Hacker et al., 2008). However, the depths at which the Vp increase relatively rapid in a short vertical extent vary among arcs (Fig. 9b). The reconstructed crustal column of the Talkeetna paleoarc exhibit an increase of P-wave velocities from 6.3 to 6.7 at a paleodepth of about 22 km, while we inferred a similar change in Valle Fértil section but located a few kilometers deeper than in Talkeetna. In the Sierra Nevada arc, a relatively sharp variation of P-wave velocities from <6.5 to >7.6 km/s is observed between 25 and 35 km below the present-day surface (Fliedner et al., 2000). However, the Sierra Nevada arc has lost some of the upper crust, as batholiths are exposed at the surface. Detrital grain studies from sediments west of the Sierra Nevada also suggest significant erosion since at least the Eocene (Cecil et al., 2010). Although the Sierra Nevada arc cannot be fully reconstructed, it is still significant to compare all the cases at the fixed depth of 28 km, which represents the deepest exhumed levels of the Valle Fértil section. The lithologies dominating the plutonic crust of the Famatinian arc have significantly higher seismic velocities than the Sierra Nevada arc crust, but much lower velocities than those that dominate active island arcs (e.g. Calvert, 2011).

7.3. The thermal structure of the Famatinian middle crust

The consistency of P–T estimates with geological constraints allows us to infer the thermal structure for middle crustal levels of the Famatinian arc found fossilized throughout central Sierra de Valle Fértil. The P–T conditions of the Sierra de Valle Fértil arc crust can be replicated with calculated steady-state 1D thermal models that use basal heat flow between 55 and 90 mW m^{-2} and radioactive heat production decreasing exponentially over a characteristic length scale of 10 km (Fig. 10a). Projected on a depth–T plot, the array of paleo P–T estimates shows an increase of the thermal gradient with decreasing paleo-depths. This perhaps reflects that the P–T conditions we have reconstructed do not exactly preserve the geothermal gradient of the active Famatinian arc. The problem might be due to the resetting of mineral compositions during slow cooling of granulite-facies rocks (Frost and Chacko, 1989; Pattison et al., 2003; Spear et al., 1999). In particular, the metasediments exposed within the mafic unit would likely have been subjected to higher temperatures for longer periods of time than metasediments within the silicic units. Thus, metasediments preserved at shallower plutonic levels may yield peak metamorphic temperature, whereas metasediments from greater depths may have cooled slowly and thus record ion-exchange closure temperatures. Nevertheless, taken together the P–T pairs recovered throughout the bulk Sierra de Valle Fértil section suggest a thermal structure comparable with geothermal profiles observed in several active and ancient magmatic arcs (Fig. 10b).

Temperatures in the lowest parts of Valle Fértil section arcs were higher than 850 °C at about 27 km. By simple extrapolation to deeper levels we infer temperature of about 1000 °C at depths between 30 and 35 km. Kelemen et al. (2003) showed that these P–T conditions beneath arcs are consistent with petrological observations and provide evidence for a thin thermal boundary layer between the mantle wedge and the base of the arc crust.

A somewhat related issue is whether the hot thermal conditions recorded at middle and upper arc crustal levels are sustained by magmatic advection of heat, or the conductive heat transfer from the hot, lower crust, or both. Thermomechanical forward modeling studies of heat distribution in arc settings predict ambient temperatures within the range of those recorded in the middle plutonic crust of the Famatinian arc. The hot zone model (e.g. Annen et al., 2006; Dufek and Bergantz, 2005) revealed that repetitive mafic magmatism ascending from the upper mantle and randomly intruding between Mohorovicic and Conrad discontinuities would progressively heat the overlying crust section. The geothermal gradients theoretically predicted by the hot zone model at a mature arc stage are similar to those retrieved through geothermobarometric estimates within the Valle Fértil crustal section (Fig. 10a).

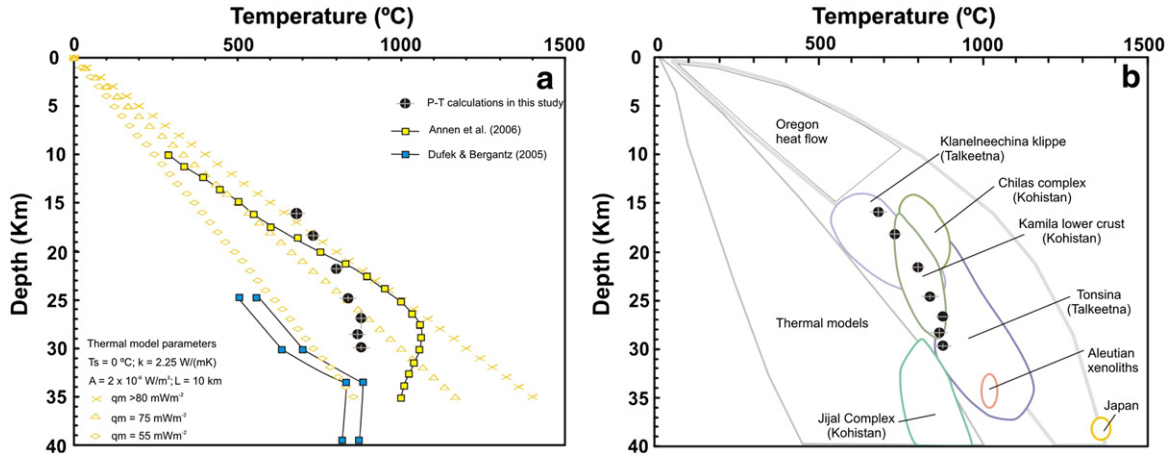

Fig. 10. (a) Steady-state continental geotherm calculated using the equation of Turcotte and Schubert (1982) and mantle heat flux for stable continental regions (55 mW m^{-2}, diamond), extensional regions (75 mW m^{-2}, triangle) and continental margins (>80 mW m^{-2}, cross). Circles represent the thermal gradient from the Sierra de Valle Fértil calculated trough petrologic P–T estimation. Yellow squares denote variation of temperature as a function of depth in a pelitic crust intruded by mafic magmatism (Annen et al., 2006). Blue squares show variation of temperature of active intrusion in a 34 km thick crust (Dufek and Bergantz, 2005). (b) Thermal gradient from the Sierra de Valle Fértil (black circles) compared to predicted geotherms from thermal modeling (gray thin line) and petrologic estimates from arcs worldwide. Thermal structure calculated to be consistent with petrological estimates (wide gray line). The thermal gradient of the deepest part of the Sierra de Valle Fértil record similar values to those inferred in ancient arcs like Kohistan and Talkeetna.
Mantle heat flux for stable continental regions, extensional regions and continental margins is after Jaupart et al. (2007); b, thermal structure calculated to be consistent with petrological estimates was taken from Kelemen et al. (2003).

8. Conclusions

Here we present the reconstruction of lower to middle arc crust preserved in the Ordovician Sierra de Valle Fértil igneous complex in northwest Argentina. Thermobarometric estimates from intercalated metasedimentary rocks are used to constrain the conditions under which the Valle Fértil igneous rocks crystallized. The preserved section is fairly continuous and exposes ~15 km of paleo thickness (~15–30 km depths). There is an overall trend toward more mafic compositions with depth as granodiorites give way to tonalites, diorites, and gabbros, and there are rather abrupt transitions separating major compositional units. Granodiorite and tonalite dominate the middle crust down to ~20 km depth, tonalites and diorites from 20 and 25 km, and gabbros from 25 and 30 km. Approximately fourteen kilometers of crust may be missing from the top of the section. From along-strike exposures of the Famatinian arc to the north, we infer this upper crustal section to comprise sediments, volcanics, and high-level plutons. Basement exposures are also not present, and so the entire thickness of the arc crust is unknown at the Valle Fértil complex. We provide estimates for the seismic wave velocity structure in order to compare the Famatina arc to other arcs, both active and ancient.

In general, the internal array of rocks for the Famatinian arc resembles that observed in other arcs (e.g. DeBari and Greene, 2011; Miller and Snoke, 2009), as P wave velocities increase step-wise with increasing depth. There are notable differences, though. The inferred silicic plutonic (P wave velocities <6.5 km/s) thickness at the Famatina is about 10 to 15 km thinner than that of typical continental arcs such as the Sierra Nevada and the Cascades. By contrast, this type of low velocity, silicic crust is much thinner at island arcs such as the Aleutians, Izu Bonin, the Marianas, and the ancient Talkeetna arc. At crustal paleodepths of ~15–24 km, the calculated P wave velocities for the Valle Fértil section are lower, in general, than those reported for other arcs (Sierra Nevada is the exception).

Our results also indicate a 10-km-thick middle to lower crust that evolved under a high geothermal gradient (25–35 °C/km). This is consistent with models advocating the addition of heat by continuously active mafic magmatic systems (Annen and Sparks, 2002; Annen et al., 2006; Dufek and Bergantz, 2005). The high thermal regime at middle crustal levels indicates the establishment of a mature arc system and requires repeated mafic magma emplacement beneath and into the crust to drive the thermal maturation. According to available geochronological data (Ducea et al., 2010), this development and maturation occurred rapidly (<20 m.y.).

Supplementary data to this article can be found online at http://dx.doi.org/10.1016/j.tecto.2012.12.032.

Acknowledgments

We acknowledge the reviewers Professors B. Hacker and O. Jagoutz for providing extremely constructive criticisms that greatly assisted the revision. We also acknowledge the journal editor Prof. Fabrizio Storti for his constructive and valuable comments that enlarge the strength of this study. Cristobal Cantero is thanked for his effort in assisting our work with JEOL EMPA at the University of Huelva, which was the primary instrument used for quantitative analyses and for obtaining several X-ray mapping one of which was chosen for this paper. This research is supported by FONCyT-Argentina grants PICT01904/07 and PICT1299/08 and by CONICET grant PIP0072. The field work was partly funded by grants of the Universidad Nacional de Río Cuarto, Argentina.

References

Aceñolaza, G.F., 2003. The Cambrian system in Northwestern Argentina: stratigraphical and palaeontological framework. Geologica Acta 1, 23–39.
Aceñolaza, F.G., Miller, H., Toselli, A.J., 2000. The Pampean and Famatinian cycles — superposed orogenic events in the West Gondwana. Zeitschrift für Angewandte Geologie, Sonderheft SH 1, 337–344.
Annen, C., Sparks, R.S.J., 2002. Effects of repetitive emplacement of basaltic intrusions on thermal evolution and melt generation in the crust. Earth and Planetary Science Letters 203, 937–955.
Annen, C., Blundy, J.D., Sparks, R.S.J., 2006. The genesis of calc-alkaline intermediate and silicic magmas in deep crustal hot zones. Journal of Petrology 47, 505–539.
Astini, R.A., 1998. Stratigraphic evidence supporting the rifting, drifting and collision of the Laurentian Precordillera terrane of western Argentina. In: Pankhurst, R.J., Rapela, C.W. (Eds.), The Proto-Andean Margin of Gondwana: Geological Society of London Special Publication, 142, pp. 11–33.
Astini, R.A., Dávila, F.M., 2004. Ordovician back arc foreland and Ocloyic thrust belt development on the western Gondwana margin as a response to Precodillera terrane accretion. Tectonics 23, TC4008 http://dx.doi.org/10.1029/2003TC001620.
Barazangi, M., Isacks, B.I., 1976. Spatial distribution of earthquakes and subduction of the Nazca plate beneath South America. Geology 4, 686–692.
Behn, M.D., Kelemen, P.B., 2006. Stability of arc lower crust: Insights from the Talkeetna arc section, south central Alaska, and the seismic structure of modern arcs. Journal of Geophysical Research 111, B11207 http://dx.doi.org/10.1029/2006JB004327.
Berman, R.G., 1988. Internally-consistent thermodynamic data for minerals in the system Na_2O–K_2O–CaO–MgO–FeO–Fe_2O_3–Al_2O_3–SiO_2–TiO_2–H_2O–CO_2. Journal of Petrology 29, 445–522.

Berman, R.G., 1990. Mixing properties of Ca–Mg–Fe–Mn garnets. American Mineralogist 75, 328–344.
Berman, R.G., Aranovich, L.Ya., 1996. Optimized standard state and solution properties of minerals. I. Model calibration for olivine, orthopyroxene, cordierite, garnet, and ilmenite in the system FeO–MgO–CaO–Al_2O_3–TiO_2–SiO_2. Contributions to Mineralogy and Petrology 126, 1–24.
Calvert, A.J., 2011. The seismic structure of island arc crust. In: Brown, D., Ryan, P. (Eds.), Arc–Continent Collision: The Making of an Orogen, Frontiers in Earth Sciences. Springer, Heidelberg.
Calvert, A.J., Klemperer, S.L., Takahashi, N., Kerr, B.C., 2008. Three-dimensional crustal structure of the Mariana island arc from seismic tomography. Journal of Geophysical Research 113 http://dx.doi.org/10.1029/2007JB004939 B01406.
Caminos, R., 1979. Sierras Pampeanas Noroccidentales. Salta, Tucumán, Catamarca, La Rioja y San Juan. In: Leanza, E.F. (Ed.), II Simposio de Geología Regional Argentina, 1. Academia Nacional de Ciencias, Córdoba, pp. 225–291.
Casquet, C., Baldo, E., Pankhurst, R.J., Rapela, C.W., Galindo, C., Fanning, C.M., Saavedra, J., 2001. Involvement of the Argentine Precordillera Terrane in the Famatinian Mobile Belt: geochronological (U–Pb SHRIMP) and metamorphic evidence from Sierra de Pie de Palo. Geology 29, 703–706.
Castro de Machuca, B., Arancibia, G., Morata, D., Belmar, M., Previley, L., Pontoriero, S., 2007. P–T–t evolution of an Early Silurian medium grade shear zone on the west side of the Famatinian magmatic arc, Argentina: implications for the assembly of the Western Gondwana margin. Gondwana Research 13, 216–226.
Cecil, M.R., Ducea, M., Reiners, P., Gehrels, G., Mulch, A., Allen, A., Campbell, I., 2010. Provenance of Eocene river sediments from the central northern Sierra Nevada and implications for paleotopography. Tectonics 29, TC6010 http://dx.doi.org/10.1029/2010TC002717, 2010.
Christensen, N.I., Mooney, W.D., 1995. Seismic velocity structure and composition of the continental crust: a global view. Journal of Geophysical Research 100, 9761–9788.
Clemens, K., Miller, H., 1996. Sedimentología, proveniencia y posición geotectónica de las sedimentitas del Precámbrico y Paleozoico inferior del Sistema de Famatina. Münchner Geologische Hefte 19A, 31–50.
Coira, B., Pérez, B., Flores, P., Kay, S.M., Woll, B., Hanning, M., 1999. Magmatic sources and tectonic setting of Gondwana margin Ordovician magmas, northern Puna of Argentina and Chile. In: Ramos, V., Keppie, J. (Eds.), Laurentia-Gondwana Connections Before Pangea: Geological Society of America, Special Paper, 336, pp. 145–170.
Collo, G., Astini, R., 2008. La Formación Achavil: una nueva unidad de bajo grado metamórfico en la evolución cámbrica superior del Famatina. Revista de la Asociación Geológica Argentina 63, 344–362.
Collo, G., Astini, R., Cawood, P.A., Buchan, C., Pimentel, M., 2009. U–Pb detrital zircon ages and Sm–Nd isotopic features in low-grade metasedimentary rocks of the Famatina belt: implications for late Neoproterozoiceearly Palaeozoic evolution of the proto-Andean margin of Gondwana. Journal of the Geological Society 166, 303–319.
Comínguez, H., Ramos, V., 1991. La estructura profunda entre Precordillera y Sierras Pampeanas de la Argentina: Evidencia de la sísmica de reflexión profunda. Revista Geológica de Chile 18, 3–14.
Cristofolini, E., Otamendi, J., Tibaldi, A., Martino, R., Baliani, I., 2010. Geología de la porción occidental de la Sierra de valle Fértil, San Juan, a partir de observaciones en la quebrada de Otarola. Revista de la Asociación Geológica Argentina 67, 521–535.
Cristofolini, E.A., Otamendi, J., Ducea, M., Pearson, D., Tibaldi, A., Balíani, I., 2012. Detrital zircon U–Pb ages of metasedimentary rocks from the Sierra de Valle Fértil: entrapment of Middle and Late Cambrian marine successions in deep roots of the Early Ordovician Famatinian arc. Journal of South American Earth Sciences 37, 77–94.
DeBari, S.M., Greene, A.R., 2011. Vertical stratification of composition, density, and inferred magmatic processes in exposed arc crustal sections. In: Brown, D., Ryan, P. (Eds.), Arc–Continent Collision: The Making of an Orogen, Frontiers in Earth Sciences. Springer, Heidelberg.
Ducea, M.N., Otamendi, J.E., Bergantz, G., Stair, K., Valencia, V., Gehrels, G.E., 2010. Timing constraints on building an intermediate plutonic arc crustal section: U–Pb zircon geochronology of the Sierra de Valle Fértil, Famatinian arc, Argentina. Tectonics 29, 1–22.
Dufek, J., Bergantz, G.W., 2005. Lower crustal magma genesis and preservation: a stochastic framework for the evaluation of basalt–crust interaction. Journal of Petrology 46, 2167–2195.
Fanning, C.M., Pankhurst, R.J., Rapela, C.W., Baldo, E.G., Casquet, C., Galindo, C., 2004. K-bentonites in the Argentine Precodillera contemporaneous with rhyolite volcanism in the Famatinian arc. Journal of the Geological Society of London 161, 747–756.
Fliedner, M.M., Klemperer, S.L., 2000. Crustal structure transition from oceanic arc to continental arc, eastern Aleutian Islands and Alaska Peninsula. Earth and Planetary Science Letters 179, 567–579.
Fliedner, M.M., Klemperer, S.L., Christensen, N.I., 2000. Three dimensional seismic model of the Sierra Nevada arc, California, and its implications for crustal and upper mantle composition. Journal of Geophysical Research 105, 10899–10921.
Frost, B.R., Chacko, T., 1989. The granulite uncertainty principle: limitations on thermobarometry in granulites. Journal of Geology 97, 435–450.
Gallien, F., Mogessie, A., Bjerg, E., Delpino, S., Castro de Machuca, B., Thöni, M., Klötzlid, U., 2010. Timing and rate of granulite facies metamorphism and cooling from multi-mineral chronology on migmatitic gneisses, Sierras de La Huerta and Valle Fértil, NW Argentina. Lithos 114, 229–252.
Hacker, B.R., Abers, G.A., 2004. Subduction Factory 3: an Excel worksheet and macro for calculating the densities, seismic wave speeds, and H_2O contents of minerals and rocks at pressure and temperature. Geochemistry, Geophysics, Geosystems 5 http://dx.doi.org/10.1029/2003GC000614 Q01005.
Hacker, B.R., Mehl, L., Kelemen, P.B., Rioux, M., Behn, M.D., Luffi, P., 2008. Reconstruction of the Talkeetna intraoceanic arc of Alaska through thermobarometry. Journal of Geophysical Research 113, B03204 http://dx.doi.org/10.1029/2007JB005208.
Holbrook, W.S., Lizarralde, D., McGreary, S., Bangs, N., Diebold, J., 1999. Structure and composition of the Aleutian island arc and implications for continental crustal growth. Geology 27, 31–34.
Holland, T., Powell, R., 1992. Plagioclase feldspars: activity–composition relations based upon Darken's quadratic formalism and Landau theory. American Mineralogist 77, 53–61.
Holland, T.J.B., Powell, R., 1998. An internally consistent thermodynamic dataset for phases of petrological interest. Journal of Metamorphic Geology 16, 309–343.
Jaupart, C., Labrosse, S., Mareschal, J.C., 2007. Temperatures, heat and energy in the mantle of the Earth. In: Schubert, G. (Ed.), Treatise on Geophysics, vol. 7. Elsevier Ltd., pp. 253–304.
Kawate, S., Arima, M., 1998. Petrogenesis of the Tanzawa plutonic complex, central Japan: exposed felsic middle crust of the Izu-Bonin-Mariana arc. Island Arc 7, 342–358.
Kelemen, P.B., Parmentier, E.M., Rilling, J., Mehl, L., Hacker, B.R., 2003. Thermal structure due to solid-state flow in the mantle wedge beneath arcs. In: Eiler, J. (Ed.), Inside the Subduction Factory, Geophys. Monogr. Ser., vol. 138. AGU, Washington D.C., pp. 293–311.
Kitamura, K., Ishikawa, M., Arima, M., 2003. Petrological model of the northern Izu-Bonin-Mariana arc crust: constraints from high-pressure measurements of elastic wave velocities of the Tanzawa plutonic rocks, central Japan. Tectonophysics 37, 213–221.
Kodaira, S., Sato, T., Takahashi, N., Miura, S., Tamura, Y., Tatsumi, Y., Kaneda, Y., 2007. New seismological constraints on growth of continental crust in the Izu-Bonin intra-oceanic arc. Geology 35, 1031–1034.
Kohn, M.J., Spear, F.S., 2000. Retrograde Net Transfer Reaction (ReNTR) insurance for P–T estimates. Geology 28, 1127–1130.
Kretz, R., 1983. Symbols for rock-forming minerals. American Mineralogist 68, 277–279.
Mángano, M.G., Buatois, L.A., 2004. Integración de estratigrafía secuencial, sedimentología e icnología para un análisis cronoestratigráfico del Paleozoico inferior del noroeste argentino. Revista de la Asociación Geológica Argentina 59, 273–280.
Mángano, M.G., Astini, R.A., Buatois, L.A., Dávila, F.M., 2003. The Ordovician System in the Famatina Belt: depositional and tectonic evolution. In: Aceñolaza, F.C. (Ed.), Aspects of the Ordovician System in Argentina: Serie Correlación Geológica, vol. 16, pp. 295–312.
Mannheim, R., Miller, H., 1996. Las rocas volcánicas y subvolcánicas eopaleozoicas del Sistema de Famatina. Münchner Geologische Hefte 19A, 159–186.
Miller, D.J., Christensen, N.I., 1994. Seismic signature and geochemistry of an island arc: a multidisciplinary study of the Kohistan accreted terrane, northern Pakistan. Journal of Geophysical Research 99, 11623–11642.
Miller, R., Snoke, A., 2009. The utility of crustal cross sections in the analysis of orogenic processes in contrasting tectonic settings. The Geological Society of America Special Paper 456.
Mirré, J.C., 1976. Descripción Geológica de la Hoja 19e, Valle Fértil, Provincias de San Juan y La Rioja. Servicio Geológico Nacional, Boletín, 147, pp. 1–70 (Buenos Aires).
Mulcahy, S.R., Roeske, S.M., McClelland, W.C., Jourdan, F., Iriondo, A., Renne, P.R., Vervoort, J.D., Vujovich, G.I., 2011. Structural evolution of a composite middle- to lower-crustal section: the Sierra de Pie de Palo, northwest Argentina. Tectonics 30, TC1005 http://dx.doi.org/10.1029/2009TC002656.
Nakanishi, A., Kurashimo, E., Tatsumi, Y., Yamaguchi, H., Miura, S., Kodaira, S., Obana, K., Takahashi, N., Tsuru, T., Kaneda, Y., Iwasaki, T., Hirata, N., 2009. Crustal evolution of the southwestern Kuril arc, Hokkaido Japan, deduced from seismic velocity and geochemical structure. Tectonophysics 472, 105–123.
Otamendi, J.E., Tibaldi, A.M., Vujovich, G.I., Viñao, G.A., 2008. Metamorphic evolution of migmatitas from the deep Famatinian arc crust exposed in Sierras Valle Fértil–La Huerta, San Juan, Argentina. Journal of South American Earth Sciences 25, 313–335.
Otamendi, J.E., Vujovich, G.I., de la Rosa, J.D., Tibaldi, A.M., Castro, A., Martino, R.D., Pinotti, L.P., 2009. Geology and petrology of a deep crustal zone from the Famatinian paleo-arc, Sierras de Valle Fértil and La Huerta, San Juan, Argentina. Journal of South American Earth Sciences 27, 258–279.
Pankhurst, R.J., Rapela, C.W., Saavedra, J., Baldo, E., Dahlquist, J., Pascua, I., Fanning, C.M., 1998. The Famatinian magmatic arc in the central Sierras Pampeanas: an Early to Mid-Ordovician continental arc on the Gondwana margin. In: Pankhurst, R.J., Rapela, C.W. (Eds.), The Proto-Andean Margin of Gondwana: Geological Society London, Special Publication, 142, pp. 43–368.
Pankhurst, R.J., Rapela, C.W., Fanning, C.M., 2000. Age and origin of coeval TTG, I- and S-type granites in the Famatinian belt of NW Argentina. Transactions of the Royal Society of Edinburgh: Earth Sciences 91, 151–168.
Parsons, T., Trehu, A.M., Luetgert, J.H., Miller, K., Kilbride, F., Wells, R.E., Fisher, M.A., Flueh, E., St Brink, U., Christensen, N.I., 1998. A new view into the Cascadia subduction zone and volcanic arc: implications for earthquake hazards along the Washington margin. Geology 26, 199–202.
Patiño Douce, A.E., Johnston, A.D., Rice, J., 1993. Octahedral excess mixing properties in biotite: a working model with applications to geobarometry and geothermometry. American Mineralogist 78, 113–131.
Pattison, D., Chacko, T., Farquhar, J., McFarlane, C., 2003. Temperatures of granulite- facies metamorphism: constraints from experimental phase equilibria and thermobarometry corrected for retrograde exchange. Journal of Petrology 44, 867–900.
Rapela, C.W., Pankhurst, R., Baldo, E., Casquet, C., Galindo, C., Fanning, C., Saavedra, J., 2001. Ordovician metamorphism in the Sierras Pampeanas: new U–Pb SHRIMP ages in central-east Valle Fértil and the Velasco batholith. Proceedings III South American Symposium on Isotope Geology, 3, pp. 616–619 (Pucón, Chile).
Rioux, M., Mattinson, J., Hacker, B., Kelemen, P., Blusztajn, J., Hanghøj, K., Gehrels, G., 2010. Intermediate to felsic middle crust in the accreted Talkeetna arc, the Alaska

Peninsula and Kodiak Island, Alaska: an analogue for low velocity middle crust in modern arcs. Tectonics 29, TC3001 http://dx.doi.org/10.1029/2009TC002541.
Robinson, P., 1991. The eye of the petrographer, the mind of the petrologist. American Mineralogist 76, 1781–1810.
Rudnick, R.L., 1995. Making continental crust. Nature 378, 571–578.
Saleeby, J., Ducea, M., Clemens-Knott, D., 2003. Production and loss of high-density batholithic root, southern Sierra Nevada, California. Tectonics 22, 1064 http://dx.doi.org/10.1029/2002TC001374.
Sobolev, S., Babeyko, A., 2004. Modeling of mineralogical composition, density and elastic wave velocities in anhydrous magmatic rocks. Surveys in Geophysics 15, 515–544 (DELING).
Spear, F.S., 1993. Metamorphic Phase Equilibria and Pressure–Temperature–Time Paths. Mineralogical Society of America, Washington, D.C.(799 pp.).
Spear, F.S., Kohn, M.J., Cheney, J.T., 1999. P–T paths from anatectic pelites. Contributions to Mineralogy and Petrology 134, 17–32.
Suyehiro, K., Takahashi, N., Ariie, Y., Yokoi, Y., Hino, R., Shinohara, M., Kanazawa, T., Hirata, N., Tokuyama, H., Taira, A., 1996. Continental crust, crustal underplating, and low-Q upper mantle beneath an oceanic island arc. Science 272, 390–392.
Taylor, S.R., McLennan, S.M., 1985. The Continental Crust: Its Composition and Evolution. Blackwell, Oxford.
Thomas, W.A., Astini, R.A., 1996. The Argentine precordillera: a traveler from the Ouachita embayment of North American Laurentia. Sciences 273, 752–757.
Tibaldi, A., Otamendi, J., Cristofolini, E., Vujovich, G., Martino, R., 2009. Condiciones de formación de gabros y migmatitas derivadas de rocas máficas en el centro de la Sierra de Valle Fértil: implicancias en la constitución del arco Famatiniano. Revista de la Asociación Geológica Argentina 65, 487–503.
Tibaldi, A.M., Álvarez-Valero, A.M., Otamendi, J.E., Cristofollini, E.A., 2011. Formation of paired pelitic and gabbroic migmatites: an empirical investigation of the consistency of geothermometers, geobarometers, and pseudosections. Lithos 122, 57–75.
Toselli, A.J., Durand, F.R., Rossi de Toselli, J.N., Saavedra, J., 1996. Esquema de evolución geotectónica y magmática Eopaleozoica del sistema de Famatina y sectores de Sierras Pampeanas. Actas XIII Congreso Geológico Argentino y III Congreso de Exploración de Hidrocarburos, 5, pp. 443–462.
Turcotte, D.L., Schubert, G., 1982. Geodynamics, Applications of Continuum physics to Geological Problems. Wiley, Canada (Ed.).
Vujovich, G.I., Ramos, V.A., 1999. Mapa geotectónico de la República Argentina (1:2.500.000). Subsecretaría de Minería de la Nación, Buenos Aires (Servicio Geológico Minero Argentino).
Vujovich, G.I., Godeas, M., Marín, G., Pezzutti, N., 1996. El complejo magmático de la Sierra de La Huerta, provincia de San Juan. Actas XIII Congreso Geológico Argentino y III Congreso de Exploración de Hidrocarburos, 3, pp. 465–475.
Vujovich, G., Pieters, P., Tchiliguirian, P., Chernicoff, J., Lyons, P., Stuart-Smith, G., Marín, G., Turel, A., 1998. Hoja Geológica 3166-III, Chepes, escala 1:250.000. Provincias de San Juan y La Rioja. Subsecretaría de Minería de la Nación, Servicio Geológico Minero Argentino, Buenos Aires, pp. 1–54.